Primordial non-Gaussianity from the large scale structure

V Desjacques[1], **U Seljak**[1,2]

[1] Institute for Theoretical Physics, University of Zürich, Winterthurerstrasse 190, CH-8057 Zürich, Switzerland
[2] Physics and Astronomy Department, University of California, and Lawrence Berkeley National Laboratory, Berkeley, California 94720, USA

E-mail: `dvince@physik.uzh.ch`, `seljak@physik.uzh.ch`

Abstract.
Primordial non-Gaussianity is a potentially powerful discriminant of the physical mechanisms that generated the cosmological fluctuations observed today. Any detection of non-Gaussianity would have profound implications for our understanding of cosmic structure formation. In this paper, we review past and current efforts in the search for primordial non-Gaussianity in the large scale structure of the Universe.

1. Introduction

In generic inflationary models based on the slow roll of a scalar field, primordial curvature perturbations are produced by the inflaton field as it slowly rolls down its potential [1, 2, 3, 4]. Most of these scenarios predict a nearly scale-invariant spectrum of adiabatic curvature fluctuations, a relatively small amount of gravity waves and tiny deviations from Gaussianity in the primeval distribution of curvature perturbations [5, 6, 7]. While the latest measurements of the cosmic microwave background (CMB) anisotropies favor a slightly red power spectrum [8], no significant detection of a *B*-mode or of primordial non-Gaussianity (NG) has thus far been reported from CMB observations.

While the presence of a *B*-mode can only be tested with CMB measurements [9, 10], primordial deviations from Gaussianity can leave a detectable signature in the distribution of CMB anisotropies *and* in the large scale structure (LSS) of the Universe. Until recently, it was widely accepted that measurement of the CMB furnish the best probe of primordial non-Gaussianity [11]. However, these conclusions did not take into account the scale-dependence of the galaxy power spectrum and bispectrum arising for primordial NG of the local $f_{\mathrm{NL}}^{\mathrm{loc}}$ type [12, 13]. These theoretical results, together with rapid developments in observational techniques that will provide large amount of LSS data, will enable us to critically confront predictions of non-gaussian models. In particular, galaxy clustering should provide independent constraints on the magnitude of primordial non-Gaussianity as competitive as those from the CMB and in the long run may even give the best constraints.

The purpose of this work is to provide an overview of the search for a primordial non-Gaussian signal in the large scale structure. We will begin by briefly summarizing how non-Gaussianity arises in inflationary models (§2). Next, we will discuss the impact of primordial non-Gaussianity on the mass distribution in the low redshift Universe (§3). The main body of this review is §4, where we describe in detail an number of methods exploiting the abundance and clustering properties of observed tracers of the LSS to constrain the amount of initial non-Gaussianity. We conclude with a discussion of present and forecasted constraints achievable with LSS surveys (§5).

2. Models and observables

Single-field slow-roll models lead to a very small level of primordial non-Gaussianity [14, 6, 7]. This is because they assume i) a single dynamical field (the inflaton) ii) canonical kinetic energy terms (i.e. perturbations propagate at the speed of light) iii) slow roll (i.e. the timescale over which the inflaton field changes is much larger than the Hubble rate) iv) an initial adiabatic Bunch-Davis vacuum. The lowest order statistics sensitive to non-Gaussian features in the initial distributions of scalar perturbations $\Phi(\mathbf{x})$ (We shall adopt the standard CMB convention in which $\Phi(\mathbf{x})$ is the Bardeen's curvature perturbation in the matter era) is the 3-point function or bispectrum $B_\Phi(\mathbf{k}_1, \mathbf{k}_2, \mathbf{k}_3)$, which is a function of any triangle $\mathbf{k}_1 + \mathbf{k}_2 + \mathbf{k}_3 = 0$ (as follows from statistical homogeneity which we assume throughout this paper). It has been shown that, in the squeezed limit $k_3 \ll k_1 \approx k_2$, the bispectrum of *any* single-field slow-roll inflationary model asymptotes to the local shape [15, 16, 17]. The corresponding nonlinear parameter predicted by these models is $f_{\mathrm{NL}}^{\mathrm{loc}} = \frac{5}{12}(1 - n_s) \approx 0.017$ where n_s is the tilt or spectral index of the power spectrum $P_\Phi(k)$, which is accurately measured

to be $n_s \approx 0.960 \pm 0.013$ [8]. Therefore, any robust measurement of $f_{\mathrm{NL}}^{\mathrm{loc}}$ well above this level would thus rule out single-field slow-roll inflation as defined above.

2.1. The shape of the primordial bispectrum

Large, potentially detectable amount of Gaussianity can be produced when at least one of the assumptions listed above is violated, i.e. by multiple scalar fields [18, 19], nonlinearities in the relation between the primordial scalar perturbations and the inflaton field [14, 7], interactions of scalar fields [20], a modified dispersion relation or a departure from the adiabatic Bunch-Davies ground state [21]. Generation of a large non-Gaussian signal is also expected at reheating [22] and in the ekpyrotic scenario [23]. Each of these physical mechanisms leaves a distinct signature in the primordial 3-point function $B_\Phi(\mathbf{k}_1, \mathbf{k}_2, \mathbf{k}_3)$, a measurement of which would thus provide a wealth of information about the physics generating the primordial fluctuations. Although the configuration shape of the primordial bispectrum can be extremely complex in some models, there are broadly three classes of shape characterizing the local, equilateral and folded type of primordial non-Gaussianity [24, 25]. The magnitude of each template "X" is controlled by a dimensionless nonlinear parameter $f_{\mathrm{NL}}^{\mathrm{X}}$ which we seek to constrain using CMB or LSS observations.

Any non-Gaussianity generated outside the horizon induces a three-point function that is peaked on squeezed or collapsed triangles for realistic values of the scalar spectral index. The resulting non-Gaussianity depends only on the local value of the Bardeen's curvature potential and can thus be conveniently parameterized up to third order by [14, 7, 11, 26]

$$\Phi(\mathbf{x}) = \phi(\mathbf{x}) + f_{\mathrm{NL}}^{\mathrm{loc}}\phi^2(\mathbf{x}) + g_{\mathrm{NL}}^{\mathrm{loc}}\phi^3(\mathbf{x}) , \tag{1}$$

where $\phi(\mathbf{x})$ is an isotropic Gaussian random field and $f_{\mathrm{NL}}^{\mathrm{loc}}$, $g_{\mathrm{NL}}^{\mathrm{loc}}$ are dimensionless, phenomenological parameters. Since curvature perturbations are of magnitude $\mathcal{O}(10^{-5})$, the cubic order correction should always be negligibly small compared to the quadratic one when $\mathcal{O}(f_{\mathrm{NL}}^{\mathrm{loc}}) \sim \mathcal{O}(g_{\mathrm{NL}}^{\mathrm{loc}})$. However, this condition is not satisfied by some multifield inflationary models such as the curvaton scenario, in which a large $g_{\mathrm{NL}}^{\mathrm{loc}}$ and a small $f_{\mathrm{NL}}^{\mathrm{loc}}$ can be simultaneously produced [19]. The quadratic term generates the 3-point function at leading order,

$$B_\Phi^{\mathrm{loc}}(\mathbf{k}_1, \mathbf{k}_2, \mathbf{k}_3) = 2f_{\mathrm{NL}}^{\mathrm{loc}} \left[P_\phi(k_1)P_\phi(k_2) + (\mathrm{cyc.}) \right] , \tag{2}$$

where (cyc.) denotes all cyclic permutations of the indices and $P_\phi(k)$ is the power spectrum of the Gaussian part $\phi(\mathbf{x})$ of the Bardeen potential. The cubic-order terms generates a trispectrum $T_\Phi(\mathbf{k}_1, \mathbf{k}_2, \mathbf{k}_3, \mathbf{k}_4)$ at leading order.

Equilateral type of non-Gaussianity, which arises in inflationary models with higher-derivative operators such as the DBI model, is well describe by the factorizable form [27]

$$B_\Phi^{\mathrm{eq}}(\mathbf{k}_1, \mathbf{k}_2, \mathbf{k}_3) = 6f_{\mathrm{NL}}^{\mathrm{eq}} \Big[-\big(P_\phi(k_1)P_\phi(k_2) + (\mathrm{cyc.})\big) - 2\big(P_\phi(k_1)P_\phi(k_2)P_\phi(k_3)\big)^{2/3} \tag{3}$$
$$+ \big(P_\phi^{1/3}(k_1)P_\phi^{2/3}(k_2)P_\phi(k_3) + (\mathrm{perm.})\big) \Big] .$$

It can be easily checked that the signal is largest in the equilateral configurations $k_1 \approx k_2 \approx k_3$, and suppressed in the squeezed limit $k_3 \ll k_1 \approx k_2$. Note that, in single-field slow-roll inflation, the 3-point function is a linear combination of the local and equilateral shape [15].

As a third template, we consider the folded or flattened shape which is maximized for $k_2 \approx k_3 \approx k_1/2$ [28]

$$B_\Phi^{\rm fol}(\mathbf{k}_1, \mathbf{k}_2, \mathbf{k}_3) = 6 f_{\rm NL}^{\rm fol}\Big[\big(P_\phi(k_1)P_\phi(k_2) + ({\rm cyc.})\big) + 3\big(P_\phi(k_1)P_\phi(k_2)P_\phi(k_3)\big)^{2/3} \tag{4}$$
$$- \big(P_\phi^{1/3}(k_1)P_\phi^{2/3}(k_2)P_\phi(k_3) + ({\rm perm.})\big)\Big] \ .$$

and approximate the non-Gaussianity due to modification of the initial Bunch-Davies vacuum in canonical single field action (although the latter peaks on squashed or collinear triangles). As in the previous example, $B_\Phi^{\rm fol}$ is suppressed in the squeezed configurations. Unlike $B_\Phi^{\rm eq}$ however, the folded shape induces a scale-dependent bias at large scales (see §4.3).

2.2. Statistics of the linear mass density field

The Bardeen's curvature potential $\Phi(\mathbf{x})$ is related to the linear density perturbation $\delta_0(\mathbf{k}, z)$ at redshift z through the relation

$$\delta_0(\mathbf{k}, z) = \mathcal{M}(k, z)\Phi(\mathbf{k}) \ , \tag{5}$$

where

$$\mathcal{M}(k, z) = \frac{2}{3}\frac{k^2 T(k)D(z)}{\Omega_{\rm m}H_0^2} \ . \tag{6}$$

Here, $T(k)$ is the matter transfer function normalized to unity as $k \to 0$, $\Omega_{\rm m}$ is the present-day matter density, $D(z)$ is the linear growth rate normalized to $1+z$. Eq.(5) is important as it provides the connection between the primeval curvature perturbations and the low redshift mass density field. n-point correlator of the linear matter density field can thus be related to those of $\Phi(\mathbf{x})$,

$$\langle \delta_0(\mathbf{k}) \cdots \delta_0(\mathbf{k}_n)\rangle = \left(\prod_{i=1}^{n}\mathcal{M}(k_i)\right)\langle\Phi(\mathbf{k}_1)\cdots\Phi(\mathbf{k}_n)\rangle \ . \tag{7}$$

Smoothing unavoidably arises when comparing observations of the large scale structure with theoretical predictions. Perturbation theory (PT), which is valid only in the weakly nonlinear regime [29], or the spherical collapse model, which ignores the strongly nonlinear internal dynamics of the collapsing regions [30, 31], require that the small-scale nonlinear fluctuations be smoothed out. For this reason, we introduce the *smoothed* linear density field δ_R,

$$\delta_R(\mathbf{k}, z) = \mathcal{M}(k, z)W_R(k)\Phi(\mathbf{k}) \equiv \mathcal{M}_R(k, z)\Phi(\mathbf{k}) \ , \tag{8}$$

where $W_R(k)$ is a (spherically symmetric) window function of characteristic radius R or mass scale M. We will assume a top-hat filter in configuration space throughout. Furthermore, since M and R are equivalent variables, we shall indistinctly use the notation δ_R and δ_M in what follows.

2.3. Topological defects models

In addition to inflationary scenarios, there is a whole class of models, known as topological defect models, in which cosmological fluctuations are sourced by an inhomogeneously distributed component which contributes a small fraction of the total energy momentum tensor [32, 33]. The density field is obtained as the convolution of a discrete set of points with a specific density profile. Defects are deeply rooted in

particle physics as they are expected to form at a phase transition. Since the early Universe may have plausibly undergone several phase transitions, it is rather unlikely that no defects at all were formed. Furthermore, high redshift tracers of the LSS may be superior to CMB at finding non-Gaussianity sourced by topological defects [34]. However, CMB observations already provide stringent limits on the energy density of a defect component [8], so we shall only minimally discuss the imprint of these scenarios in the large scale structure.

3. Evolution of the matter density field with primordial NG

In this Section, we summarize a number of results relative to the effect of primordial NG on the mass density field. These will be useful to understand the complexification that arises when considering biased tracers of the density field (see §4).

3.1. Setting up non-Gaussian initial conditions

Investigating the impact of non-Gaussian initial conditions (ICs) on the large scale structure traced by galaxies etc. requires simulations large enough so that many long wavelength modes are sampled. At the same time, the simulations should resolve the dark matter halos hosting the observed galaxies or quasars (QSOs), so that one can construct halo samples whose statistical properties mimic as closely as possible those of the real data. This favors the utilization of pure N-body simulations, for which a larger dynamical range can be achieved, rather than computationally more expensive hydrodynamical simulations.

The evolution of the matter density field with primordial non-Gaussianity has been studied in series of large cosmological N-body simulations seeded with Gaussian and non-Gaussian initial conditions, see e.g. [35, 36, 37, 38, 39, 40, 41, 13, 42, 43, 44]. For generic non-Gaussian (scalar) random fields, we face the problem of setting up numerical simulations with a prescribed correlation structure [45]. For the equilateral and folded type of non-Gaussianity, this task is not easily accomplished (because it requires the calculation of a number of convolutions which are computationally demanding). However, for primordial NG described by a local mapping such as the $f_{\rm NL}^{\rm loc}$ model, this is a rather straightforward operation. This is the reason why most numerical studies of structure formation with inflationary NG have so far implemented the local shape solely.

3.2. Mass density probability distribution

In the absence of primordial NG, the probability distribution function (PDF) of the initial smoothed density field, i.e. the probability that a randomly placed cell of volume V has some specific density, is Gaussian. Namely, all normalized or reduced *smoothed* cumulants S_J of order $J \geq 3$ are zero. An obvious signature of primordial NG would thus be an initially non-vanishing skewness $S_3 = \langle \delta_R^3 \rangle_c / \langle \delta_R^2 \rangle^2$ or kurtosis $S_4 = \langle \delta_R^4 \rangle_c / \langle \delta_R^2 \rangle^3 - 3/\langle \delta_R^2 \rangle$ [37, 46, 47]. Here, the subscript c denotes the connected piece of the n-point moment that cannot be simplified into a sum over products of lower order moments. At third order for instance, the cumulant of the smoothed density field is an integral of the 3-point function,

$$\langle \delta_R^3 \rangle = \int \frac{d^3 k_1}{(2\pi)^3} \int \frac{d^3 k_2}{(2\pi)^3} \int \frac{d^3 k_3}{(2\pi)^3} \, B_R(\mathbf{k}_1, \mathbf{k}_2, \mathbf{k}_3, z) \,, \qquad (9)$$

where

$$B_R(\mathbf{k}_1, \mathbf{k}_2, \mathbf{k}_3, z) = \mathcal{M}_R(k_1, z)\mathcal{M}_R(k_2, z)\mathcal{M}_R(k_3, z)B_\Phi(\mathbf{k}_1, \mathbf{k}_2, \mathbf{k}_3) \qquad (10)$$

is the bispectrum of the smoothed linear density fluctuations at redshift z. Note that, while $S_3(R, z) \propto D(z)^{-1}$, the product $\sigma S_3(R)$ does not depend on redshift. Over the range of scale $0.1 \lesssim R \lesssim 100\ h^{-1}\text{Mpc}$ accessible to LSS observations, $\sigma S_3^{(1)}(R) \equiv \sigma S_3(R, f_{\text{NL}}^{\text{X}} = 1)$ is a weakly monotonically decreasing function of R that is of magnitude $\sim 10^{-4}$ for the local, equilateral and folded templates discussed above. Strictly speaking, all reduced moments should be specified to fully characterise the density PDF, but a reasonable description of the density distribution can be achieved with moments up to the fourth order.

Numerical and analytic studies generally find that a density PDF initially skewed towards positive values produces more overdense regions, whereas a negatively skewed distribution produces larger voids. Gravitational instabilities also generate a positive skewness in the density field, reflecting the fact that the evolved density distribution exhibits an extended tail towards large overdensities [48, 49, 50, 51, 52, 53]. This gravitationally-induced signal eventually dominates the primordial contribution such that, at fixed normalization amplitude, non-Gaussian scenarios deviate more strongly from the fiducial Gaussian model at high redshift. More precisely, the time evolution of the normalized cumulants S_J can be worked out for generic Gaussian and non-Gaussian ICs using PT, or the simpler spherical collapse approximation. For Gaussian ICs, PT predicts that the normalized cumulants be time-independent to lowest non-vanishing order, with a skewness $S_3 \approx 34/7$, whereas for non-Gaussian ICs, the linear contribution to the cumulants decays as $S_J(R, z) = S_J(R, \infty)/D^{J-2}(z)$ [54, 55, 56, 57].

The persistence of the primordial hierarchical amplitude $S_J(R, \infty)$ sensitively depends upon the magnitude of S_N, $N \geq J$, relative to unity. For example, an initially large non-vanishing kurtosis could source skewness with a time-dependence and amplitude similar to that induced by nonlinear gravitational evolution [54]. Although there is an infinite class of non-Gaussian models, we can broadly divide them into weakly and strongly non-Gaussian. In weak NG models, the primeval signal in the normalized cumulants is rapidly obliterated by gravity-induced non-Gaussianity. This is the case of hierarchical scaling models where n-point correlation functions satisfy $\xi_n \propto \xi_2^{n-1}$ with $\xi_2 \ll 1$ at large scales. By contrast, strongly NG initial conditions dominate the evolution of the normalized cumulants. This occurs when the hierarchy of correlation functions obeys the dimensional scaling $\xi_n \propto \xi_2^{n/2}$, which arises in the particular case of χ^2 initial conditions [58] or in defect models such as texture [59, 38, 60]. These scaling laws have been successfully confronted with numerical investigations of the evolution of cumulants [38, 39].

Although gravitational clustering tends to erase the memory of initial conditions, numerical simulations of non-Gaussian initial conditions show that the occurrence of highly underdense and overdense regions is very sensitive to the presence of primordial NG. In fact, the imprint of primordial NG is best preserved in the low density tail of the PDF $P(\rho|R)$ of the evolved density field ρ smoothed at scale R [41, 61]. A satisfactory description of this measurement can be obtained from an Edgeworth expansion of the initial mass density field. At high densities $\rho \gg 1$, the non-Gaussian modification approximately scales as $\rho^{3/5}$ whereas, at low densities $\rho \simeq 0$, the deviation is steeper and behaves as $\rho^{6/5}$ [62].

3.3. Power spectrum and bispectrum

Primordial non-Gaussianity also imprints a signature in Fourier space statistics of the matter density field as positive values of $f_{\rm NL}^{\rm X}$ tend to increase the small scale matter power spectrum $P_\delta(k)$ [12, 41, 63] and the large scale matter bispectrum $B_\delta(\mathbf{k}_1, \mathbf{k}_2, \mathbf{k}_3)$ [12, 64].

In the weakly nonlinear regime where 1-loop PT applies, the Fourier mode of the density field for growing-mode initial conditions reads [49, 65]

$$\delta(\mathbf{k}, z) = \delta_0(\mathbf{k}, z) + \int \frac{d^3 q_1}{(2\pi)^3} \frac{d^3 q_2}{(2\pi)^3} \, \delta_{\rm D}(\mathbf{k} - \mathbf{q}_1 - \mathbf{q}_2) F_2(\mathbf{q}_1, \mathbf{q}_2) \delta_0(\mathbf{q}_1, z) \delta_0(\mathbf{q}_2, z) \, . \quad (11)$$

The kernel $F_2(\mathbf{k}_1, \mathbf{k}_2) = 5/7 + \mu(k_1/k_2 + k_2/k_1)/2 + 2\mu^2/7$, where μ is the cosine of the angle between $\mathbf{k}_1$ and $\mathbf{k}_2$, describes the nonlinear 2nd order evolution of the density field. It is nearly independent of $\Omega_{\rm m}$ and Ω_Λ and vanishes in the (squeezed) limit $\mathbf{k}_1 = -\mathbf{k}_2$. At 1-loop PT, the second term in the right-hand side of Eq.(11) generates a correction to the mass power spectrum,

$$P_\delta^{\rm NG}(k, z) = P_0(k, z) + \left[P_{(22)}(k, z) + P_{(13)}(k, z) \right] + \Delta P_\delta^{\rm NG}(k, z) \, . \, (12)$$

Here, $P_0(k)$ is the linear matter power spectrum at redshift z, $P_{(22)}$ and $P_{(13)}$ are the standard one-loop contributions in the case of Gaussian ICs [65, 66], and

$$\Delta P_\delta^{\rm NG}(k, z) = 2 \int \frac{d^3 q}{(2\pi)^3} F_2(\mathbf{q}, \mathbf{k} - \mathbf{q}) B_0(-\mathbf{k}, \mathbf{q}, \mathbf{k} - \mathbf{q}, z) \quad (13)$$

is the correction due to primordial NG [63]. This last term scales as $D^3(z)$ such that the effect of non-Gaussianity is largest at low redshift. Most importantly, $F_2(\mathbf{k}_1, \mathbf{k}_2)$ vanishes in the limit $\mathbf{k}_1 = -\mathbf{k}_2$ as a consequence of the causality of gravitational instability. This strongly suppresses Eq. (13) at small wavenumbers, even in the local $f_{\rm NL}^{\rm loc}$ model for which $B_0(-\mathbf{k}, \mathbf{q}, \mathbf{k} - \mathbf{q})$ is maximized in the squeezed limit $|\mathbf{k}| \to 0$. For $f_{\rm NL}^{\rm loc} \sim \mathcal{O}(10^2)$, the magnitude of the correction is at a per cent level in the weakly nonlinear regime $k \lesssim 0.1 \ h{\rm Mpc}^{-1}$, in good agreement with simulations [42, 44, 67]. Extensions of the renormalization group description of dark matter clustering [68] to non-Gaussian initial density and velocity perturbations can improve the agreement up to wavenumbers $k \lesssim 0.25 \ h{\rm Mpc}^{-1}$ [69, 70].

To second order in PT, the matter bispectrum $B_\delta(k_1, k_2, k_3)$ is the sum of a primordial contribution and of two terms induced by gravitational instability [49, 71] (Here and henceforth we omit the explicit z-dependence for brevity),

$$B_\delta(\mathbf{k}_1, \mathbf{k}_2, \mathbf{k}_3) = B_0(\mathbf{k}_1, \mathbf{k}_2, \mathbf{k}_3) + \left[2 F_2(\mathbf{k}_1, \mathbf{k}_2) P_0(k_1) P_0(k_2) + ({\rm cyc.}) \right]$$

$$+ \int \frac{d^3 q}{(2\pi)^3} \left[F_2(\mathbf{q}, \mathbf{k}_3 - \mathbf{q}) T_0(\mathbf{q}, \mathbf{k}_3 - \mathbf{q}, \mathbf{k}_1, \mathbf{k}_2) + ({\rm cyc.}) \right] , \quad (14)$$

where $T_0(\mathbf{k}_1, \mathbf{k}_2, \mathbf{k}_3, \mathbf{k}_4)$ is the primordial trispectrum of the density field. Note that a similar expression can be derived for the matter trispectrum, which turns out to be less sensitive to gravitationally induced nonlinearities [72]. The reduced bispectrum Q_3 is conveniently defined as

$$Q_3(\mathbf{k}_1, \mathbf{k}_2, \mathbf{k}_3) = \frac{B_\delta(\mathbf{k}_1, \mathbf{k}_2, \mathbf{k}_3)}{\left[P_\delta(k_1) P_\delta(k_2) + {\rm cyclic} \right]} \, . \quad (15)$$

For Gaussian initial conditions, Q_3 is independent of time and, at tree-level PT, is constant and equal to $Q_3(k, k, k) = 4/7$ for equilateral configurations [49]. For general

triangles moreover, it approximately retains this simple behavior, with a dependence on triangle shape through $F_2(\mathbf{k}_1, \mathbf{k}_2)$ [12]. The inclusion of 1-loop corrections greatly improves the agreement with the numerical data [73]. An important feature property of the matter bispectrum is the fact that the primordial part scales as $Q_3 \propto 1/\mathcal{M}_R(k)$ for approximately equilateral triangles and under the assumption that $f_{\rm NL}^{\rm loc}$ is scale-independent [12]. This "anomalous" scaling considerably raises the ability of the matter bispectrum to constrain primordial NG of the local $f_{\rm NL}^{\rm loc}$ type. Unfortunately, neither the matter bispectrum nor the power spectrum are directly observable with the large scale structure of the Universe. Temperature anisotropies in the redshifted 21cm background from the pre-reionization epoch could in principle furnish a direct measurement of these quantities [74, 75, 76], but foreground contamination may severely hamper any detection. Weak lensing is another direct probe of the dark matter, although we can only observe it in projection along the line of sight [77].

As we will see shortly however, a similar scaling is also present in the power spectrum and bispectrum of observable tracers of the large scale structure such as galaxies. It is this unique signature that will make future all-sky LSS surveys competitive with forthcoming CMB experiments.

4. LSS probe of primordial non-Gaussianity

Discrete and continuous tracers of the large scale structure such as galaxies, the Lyα forest, the 21cm hydrogen line etc., provide a distorted image of the matter density field. In CDM cosmologies, galaxies form inside overdense regions [78] and this introduces a bias between the matter and galaxy distributions [79]. As a result, distinct samples of galaxies trace the matter distribution differently, the most luminous galaxies preferentially residing in the most massive DM halos. This biasing effect, which concerns most tracers of the large scale structure, is still poorly understood. Models of galaxy clustering assume for instance that the galaxy biasing relation only depends on the local mass density, but the actual biasing could be more complex [80, 81]. Because of biasing, tracers of the large scale structure will be affected by primordial non-Gaussianity in a different way than the mass density field. In this Section, we describe a number of methods exploiting the abundance and clustering properties of biased tracers to constrain the level of primordial NG. We focus on galaxy clustering as it provides the tightest limits on primordial NG (see §5).

4.1. Halo finding algorithm

Locating groups of bound particles, or DM halos, in simulations is central to the methods described below. In practice, one aims at extracting halo catalogs with statistical properties similar to those of observed galaxies or QSOs. This, however, proves to be quite difficult because the relation between observed galaxies and halos is somewhat uncertain. Furthermore, there is freedom at defining a halo mass.

A important ingredient is the choice of the halo identification algorithm. There are two categories of halo finder: i) spherical overdensity (SO) finder [82] with overdensity threshold $\Delta_{\rm vir}(z) \sim 200$ and ii) Friends-of-Friends (FOF) finder with a linking length $b \sim 0.15 - 0.2$ [83]. The mass of a SO halo is defined by the radius at which the inner overdensity exceeds $\Delta_{\rm vir}(z)$ times the background density $\bar{\rho}(z)$, whereas the mass of a FOF halo is the number of linked particles. Here, we will present results mostly for SO halos, as their mass estimate is more closely connected to the predictions of

the spherical collapse model, on which most of the analytic formulae presented in this Section are based. The question of how the spherical overdensity masses can be mapped onto friends-of-friends masses remains a matter of debate [84]. Clearly however, since the peak height depends on the halo mass M through the variance $\sigma(M)$, any systematic difference will be reflected in the value of ν associated to a specific halo sample.

4.2. Abundances of voids and bound objects

A departure from Gaussianity can significantly affect the abundance of highly biased tracers of the mass density field, as their frequency sensitively depends upon the tails of the initial density PDF [85, 86, 87]. The (extended) Press-Schechter approach has been extensively applied to ascertain the magnitude of this effect. Because it depends only on the skewness, it is weakly sensitive to the shape of the primordial bispectrum.

4.2.1. Press-Schechter approach The Press-Schechter theory [88] and its extentions based on excursion sets [89, 90, 91] predict that the number density $n(M, z)$ of halos of mass M at redshift z is entirely specified by a multiplicity function $f(\nu)$,

$$n(M, z) = \frac{\bar{\rho}}{M^2} f(\nu) \frac{d \ln \nu}{d \ln M} \ , \tag{16}$$

where the peak height $\nu(M, z) = \delta_c(z)/\sigma(M)$ is the typical amplitude of fluctuations that produce those halos. Here and henceforth, $\sigma(M)$ denotes the variance of the initial density field δ_M smoothed on mass scale $M \propto R^3$ and linearly extrapolated to present epoch, whereas $\delta_c(z) \approx 1.68 D(0)/D(z)$ is the critical linear overdensity for (spherical) collapse at redshift z. In the standard Press-Schechter approach, $n(M, z)$ is related to the level excursion probability $P(> \delta_c, M)$ that the linear density contrast of a region of mass M exceeds $\delta_c(z)$,

$$f(\nu) = -2 \frac{\bar{\rho}}{M} \frac{dP}{dM} = \sqrt{\frac{2}{\pi}} \nu \, e^{-\nu^2/2} \tag{17}$$

where the last equality assumes Gaussian initial conditions. The factor of 2 is introduced to account for the contribution of low density regions embedded in overdensities at scale $> M$. In the extended Press-Schechter theory, δ_M evolves with the mass scale M and $f(\nu)$ is the probability that a trajectory is absorbed by the constant barrier $\delta = \delta_c$ (as is appropriate in the spherical collapse approximation) on mass scale M. In general, the exact form of $f(\nu)$ depends on the barrier shape [92] and the filter shape [93]. Note also that $\int d \ln \nu \, f(\nu) = 1$, which ensures that all the mass is contained in halos.

Despite the fact that the Press-Schechter mass function overpredicts (underpredicts) the abundance of low (high) mass objects, it can be used to estimate the fractional deviation from Gaussianity. In this formalism, the non-Gaussian fractional correction to the multiplicity function is $R(\nu, f_{\mathrm{NL}}^{\mathrm{X}}) \equiv f(\nu, f_{\mathrm{NL}}^{\mathrm{X}})/f(\nu, 0) = (dP/dM)(> \delta_c, M, f_{\mathrm{NL}}^{\mathrm{X}})/(dP/dM)(> \delta_c, M, 0)$, which is readily computed once the non-Gaussian density PDF $P(\delta_M)$ is known. In the simple extensions proposed by [94] and [95], $P(\delta_M)$ is expressed as the inverse transform of a cumulant generating function. In [95], the saddle-point technique is applied directly to $P(\delta_M)$. The resulting Edgeworth expansion is then used to obtain $P(> \delta_c, M)$. Neglecting cumulants beyond the skewness, one obtain

$$R_{\mathrm{LV}}(\nu, f_{\mathrm{NL}}^{\mathrm{X}}) \approx 1 + \frac{1}{6} \sigma S_3 \left(\nu^3 - 3\nu \right) - \frac{1}{6} \frac{d \left(\sigma S_3 \right)}{d \ln \nu} \left(\nu - \frac{1}{\nu} \right) \tag{18}$$

after integration over regions above $\delta_c(z)$. In [94], it is the level excursion probability $P(> \delta_c, M)$ that is calculated within the saddle-point approximation. This approximation asymptotes to the exact large mass tail, which exponentially deviates from the Gaussian tail. To enforce the normalization of the resulting mass function, one may define $\nu_\star = \delta_\star/\sigma$ with $\delta_\star = \delta_c\sqrt{1 - S_3\delta_c/3}$, and use [94, 96]

$$\nu_\star f(\nu_\star) = M^2 \frac{n_{\mathrm{NG}}(M, z)}{\bar{\rho}} \frac{d\ln M}{d\ln \nu_\star} . \tag{19}$$

The fractional deviation from the Gaussian mass function then becomes

$$R_{\mathrm{MVJ}}(\nu, f_{\mathrm{NL}}^{\mathrm{X}}) \approx \exp\left(\frac{\nu^3}{6}\sigma S_3\right)\left[-\frac{\sigma\nu^2}{6\nu_\star}\frac{dS_3}{d\ln\nu} + \frac{\nu_\star}{\nu}\right] . \tag{20}$$

Both formulae have been shown to give reasonable agreement with numerical simulations of non-Gaussian cosmologies [97, 42, 98] (but note that [99, 13] have reached somewhat different conclusions). Expanding $\delta_\star = \delta_c\sqrt{1 - S_3\delta_c/3}$ at the first order shows that these two theoretical expectations differ in the coefficient of the $\nu\sigma S_3$ term. Therefore, it is also instructive to consider the approximation [100]

$$R(\nu, f_{\mathrm{NL}}^{\mathrm{X}}) \approx \exp\left(\frac{\nu^3}{6}\sigma S_3\right)\left[1 - \frac{\nu}{2}\sigma S_3 - \frac{\nu}{6}\frac{d(\sigma S_3)}{d\ln\nu}\right] , \tag{21}$$

which is designed to match better the Edgeworth expansion of [95] when the peak height is $\nu \sim 1$. Note that, when the primordial trispectrum is large (which, in the local model, would happen if $g_{\mathrm{NL}}^{\mathrm{loc}} \sim 10^6$), terms involving the kurtosis should also be included [94, 95, 100, 101]. In this case, it is also important to take into account a possible renormalization of the fluctuation amplitude, $\sigma_8 \to \sigma_8 + \delta\sigma_8$, to which the high mass tail of the mass function is exponentially sensitive [100]. Finally, note also that [13, 43] parametrize the fractional correction using N-body simulations.

Figure 1 shows the effect of primordial NG of the local $f_{\mathrm{NL}}^{\mathrm{loc}}$ type on the halo mass function. The dotted-dashed curve represents the approximation Eq.(21). While the agreement is reasonable for the SO halos (top panel), the theory significantly overestimates the deviation measured in the FOF mass function with linking length $b = 0.2$ (middle panel). A similar effect is noted in [98], who makes the replacement $\delta_c \to \delta_c\sqrt{q}$ with $q \approx 0.75$ to fit their measurement of $R(\nu, f_{\mathrm{NL}}^{\mathrm{loc}})$ based on FOF halos. References [102, 103] provide a physical motivation of this replacement by demonstrating that the diffusive nature of the collapse barrier introduces a similar factor. However, an overlooked but important fact is that the FOF and SO mass estimates systematically deviate from each other. In Fig.1 in particular, the FOF mass is on average 20% larger than the SO mass. As shown in the bottom panel of Fig. 1, rescaling the FOF mass to account for this difference removes most of the discrepancy with the FOF data. This illustrates an important point: the impact of primordial NG on the statistics of DM halos is sensitive to systematics caused by the choice of the halo finder. As we will see below, this may also be true for the non-Gaussian halo bias.

More sophisticated formulations based on extended Press-Schechter (EPS) theory and/or modifications of the collapse criterion look promising since they can reasonably reproduce both the Gaussian halo counts and the dependence on $f_{\mathrm{NL}}^{\mathrm{X}}$ [102, 104, 105]. The probability of first upcrossing can, in principle, be derived for any non-Gaussian density field and any choice of smoothing filter [106, 107]. For a general filter, the non-Markovian dynamics generates additional terms in the non-Gaussian correction
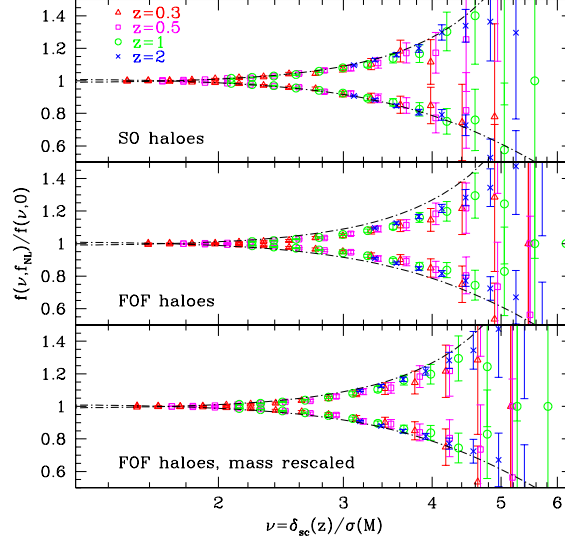
Figure 1. Fractional deviation from the Gaussian mass function as a function of the peak height $\nu = \delta_c/\sigma$. Different symbols refer to different redshifts as indicated. The solid curve is the theoretical prediction Eq. (21) at $z = 0$ based on an Edgeworth expansion of the dark matter probability distribution function. In the top panel, halos are identified using a spherical overdensity (SO) finder with a redshift-dependent overdensity threshold $\Delta_{\rm vir}(z)$. In the middle panel, a Friends-of-Friends (FOF) finding algorithm with linking length $b = 0.2$ is used. The bottom panel shows the effect of decreasing the FOF mass by 20% (see text). In all panels, error bars denote Poisson errors. For illustration, $M = 10^{15}$ M$_\odot/h$ corresponds to $\nu = 3.2$, 5.2, 7.7 at redshift $z = 0$, 1 and 2, respectively. Similarly, $M = 10^{14}$ M$_\odot/h$ and 10^{13} M$_\odot/h$ correspond to $\nu = 1.9$, 3, 4.5 and 1.2, 1.9, 2.9 respectively.

to the mass function that arise from 3-point correlators of the smoothed density δ_M at different mass scales [102]. However, large error bars still make difficult to test for the presence of such sub-leading terms. For generic moving barriers $B(\sigma)$ such as those appearing in models of triaxial collapse [108, 109], the leading contribution to the non-Gaussian correction approximately is [104]

$$R(\nu, f_{\rm NL}^{\rm X}) \approx 1 + \frac{1}{6}\,\sigma S_3\, H_3\Big(\frac{B(\sigma)}{\sigma}\Big)\,, \tag{22}$$

where $H_3(\nu) \equiv \nu^3 - 3\nu$, and agrees well with the observed deviation [105].

4.2.2. Clusters abundance   Rich clusters of galaxies trace the rare, high-density peaks in the initial conditions and thus offer the best probe of the high mass tail of the multiplicity function. To infer the cluster mass function, the X-ray and millimeter windows are better suited than the optical-wave range because selection effects can be understood better.

Following early theoretical [110, 85, 111, 86, 112] and numerical [113, 114, 36, 115] work on the effect of non-Gaussian initial conditions on the multiplicity function of cosmic structures, the abundance of clusters and X-ray counts in non-Gaussian cosmologies has received much attention in the literature. At fixed normalization

of the observed abundance of local clusters, the proto-clusters associated with high redshift $(2 < z < 4)$ Lyα emitters are much more likely to develop in strongly non-Gaussian models than in the Gaussian paradigm [40, 116, 99]. Considering the redshift evolution of cluster abundances can thus break the degeneracy between the initial density PDF and the background cosmology. In this regards, simple extensions of the Press-Schechter formalism (similar to those considered above) have been shown to capture reasonably well the cluster mass function over a wide range of redshift for various non-Gaussian scenarios [117]. Scaling relations between the cluster mass, X-ray temperature and Compton y-parameter calibrated using theory, observations and detailed simulations of cluster formation [118, 119], can then be exploited to predict the observed distribution functions of X-ray and SZ signals and assess the capability of cluster surveys to test the nature of the initial conditions [120, 121, 122, 123, 124, 125, 126, 127, 128].

An important limitation of this method is that, for a realistic amount of primordial NG, the non-Gaussian signal imprinted in cluster abundances is small compared to the systematics plaguing current and upcoming surveys [129, 130, 131]. Given the current uncertainties in the redshift evolution of clusters (one commonly assumes that clusters are observed at the epoch they collapse [130]), the selection effects in the calibration of X-ray and SZ fluxes with halo mass, the freedom in the definition of the halo mass, the degeneracy with the normalization amplitude σ_8 (for positive $f_{\rm NL}^{\rm X}$, the mass function is more enhanced at the high mass end, and this is similar to an increase in the amplitude of fluctuations σ_8 [132]) and the low number statistics, the prospects of using the cluster mass function only to place competitive limits on $f_{\rm NL}^{\rm X}$ with the current data are small. A two-fold improvement in cluster mass calibration is required to provide constraints comparable to CMB measurements [131].

4.2.3. Voids abundance The frequency of cosmic voids, which is strongly sensitive to the low density tail of the initial mass PDF, offers another probe of non-Gaussian initial conditions [133]. The Press-Schechter formalism can also be applied to ascertain the magnitude of this effect. Voids are defined as regions of mass M whose density is less than some critical value $\delta_v \leq 0$ or, alternatively, as regions for which the three eigenvalues of the tidal tensor [134] lie below some critical value $\lambda_v \leq 0$ [133, 62, 135, 105]. An important aspect in the calculation of the mass function of voids is the over-counting of voids located inside collapsing regions. This voids-in-clouds problem, as identified by [136]), can be solved within the excursion set theory by studying a two barriers problem: δ_c for halos and δ_v for voids. Including this effect reduces the frequency of the smallest voids [105]. Neglecting this complication notwithstanding, the differential number density of voids of radius R is [133, 135]

$$\frac{dn}{dR} \approx \frac{9}{2\pi^2} \sqrt{\frac{\pi}{2}} \frac{|\nu_v|}{R^4} e^{-\nu_v^2/2} \frac{d\ln|\nu_v|}{d\ln M} \left[1 - \frac{1}{6}\sigma S_3 H_3\left(|\nu_v|\right) \right], \qquad (23)$$

where $\nu_v = \delta_v/\sigma_M$. While a positive $f_{\rm NL}^{\rm X}$ produces more massive halos, it generates fewer large voids [133, 105]. Hence, the effect is qualitatively different from a simple rescaling of the normalization amplitude σ_8. A joint analysis of both abundances of clusters and cosmic voids might thus provide interesting constraints on the shape of the primordial 3-point function. There are, however, several caveats to this method, including the fact that there is no unique way to define voids [133, 137]. Clearly, voids identification algorithms will have to be tested on numerical simulations [138] before a robust method can be applied to real data.

4.3. Galaxy 2-point correlation

In Gaussian cosmologies, correlations of galaxies and clusters can be amplified relative to the mass distribution [79]. Before this was realized, it was argued that primeval fluctuations need to be non-Gaussian [139, 140] to explain the observed strong correlation of Abell clusters [141, 142]. Along these lines, [143] pointed out that primordial non-Gaussianity could significantly increase the amplitude of the two-point correlation of galaxies and clusters on large scales, However, except from [144] who showed that correlations of high density peaks in non-Gaussian models are significantly stronger than in the Gaussian model with identical mass power spectrum, subsequent work focused mostly on abundances (§4.2) or higher order statistics such as the bispectrum (§4.4). It is only recently that [13] have demonstrated the strong scale-dependent bias arising in non-Gaussian models of the local $f_{\rm NL}^{\rm loc}$ type.

4.3.1. The non-Gaussian bias In the original derivation of [13], the Laplacian is applied to the left and right hand side of $\Phi = \phi + f_{\rm NL}^{\rm loc}\phi^2$ to show that, upon substitution of the Poisson equation, the overdensity in the neighborhood of density peaks is spatially modulated by a factor proportional to the local value of ϕ. Taking into account the coherent motions induced by gravitational instabilities, the scale-dependent bias correction reads

$$\Delta b_\kappa(k, f_{\rm NL}^{\rm loc}) = 3 f_{\rm NL}^{\rm loc}\big[b_1(M) - 1\big]\delta_{\rm c}(0)\frac{\Omega_{\rm m}H_0^2}{k^2 T(k)D(z)} \ , \tag{24}$$

where $b_1(M)$ is the linear, Gaussian halo bias. The original result of [13] missed out a multiplicative factor of $T(k)^{-1}$ which was introduced subsequently by [145] upon a derivation of Eq. (24) in the limit of high density peaks. The peak-background split approach [146, 147, 92] promoted by [148] shows that the scale-dependent bias applies to any tracer of the matter density field whose (Gaussian) multiplicity function depends on the local mass density only. In this approach, the Gaussian piece of the potential is decomposed into short- and long-wavelength modes, $\phi = \phi_l + \phi_s$. This provides an intuitive explanation of the effect in terms of a local rescaling of the small-scale amplitude of matter fluctuations by a factor $1 + 2f_{\rm NL}^{\rm loc}\phi_l$ (see also [13, 149, 67]). As emphasized in [13], the scale-dependence arises from the fact that the non-Gaussian curvature perturbations $\Phi(\mathbf{x})$ are related to density fluctuations through the Poisson equation (5). There is no such effect in the χ^2 model [150, 11] nor in texture-seeded cosmologies [151] for instance.

The derivation of [145], based on the clustering of regions of the smoothed density field δ_M above threshold $\delta_c(z)$, is formally valid for high density peaks only. However, it is general enough to apply to any shape of primordial bispectrum [152]. In the high threshold limit $\nu \gg 1$, the 2-point correlation function of the level excursion set can be expressed as [110]

$$\xi_{>\nu}(\mathbf{r}) = -1 + \exp\left\{\sum_{n=2}^{\infty}\sum_{j=1}^{n-1}\frac{\nu^n \sigma^{-n}}{j!(n-j)!}\xi_R^{(n)}\left(\begin{array}{cc}\mathbf{x}_1,\cdots,\mathbf{x}_1, & \mathbf{x}_2,\cdots,\mathbf{x}_2 \\ j \text{ times} & (n-j) \text{ times}\end{array}, z=0\right)\right\} , \tag{25}$$

where $\mathbf{r} = \mathbf{x}_1 - \mathbf{x}_2$. For most non-Gaussian models in which the primordial 3-point function is the dominant correction, this expansion can be truncated at the third order and Fourier transformed to yield the non-Gaussian correction $\Delta P_{>\nu}(k)$ to the power spectrum. Assuming a small level of primordial NG, we can also write

$\Delta P_{>\nu}(k) \approx 2b_{\rm L}\Delta b_\kappa P_R(k)$, where $b_{\rm L} = b_1(M) - 1 \approx \nu^2/\delta_{\rm c}$ is the Lagrangian bias, and eventually obtain

$$\Delta b_\kappa(k, f_{\rm NL}^{\rm X}) \equiv b_\phi(k)\mathcal{F}(k, f_{\rm NL}^{\rm X}) = \left(\frac{2b_{\rm L}\delta_{\rm c}(z)}{\mathcal{M}_R(k,0)}\right)\mathcal{F}(k, f_{\rm NL}^{\rm X}) . \tag{26}$$

The dependence on the shape of the 3-point function is encoded in the function $\mathcal{F}(k, f_{\rm NL}^{\rm X})$ [145, 152],

$$\mathcal{F}(k, f_{\rm NL}^{\rm X}) = \frac{1}{16\pi^2\sigma^2}\int_0^\infty dk_1\, k_1^2 \mathcal{M}_R(k_1,0) \int_{-1}^{+1} d\mu\, \mathcal{M}_R(\sqrt{\alpha},0)\frac{B_\Phi(k_1, \sqrt{\alpha}, k)}{P_\Phi(k)} , \tag{27}$$

where $\alpha^2 = k^2 + k_1^2 + 2\mu k k_1$. Note that, for $f_{\rm NL}^{\rm X} < 0$, this fist order approximation always breaks down at sufficiently small k because $\Delta P_{>\nu}(k) < 0$.

The scale-dependent bias induced by the equilateral and folded bispectrum shape is computed in [152]. To get insights into the large scale behavior of $\Delta b_\kappa(k, f_{\rm NL}^{\rm X})$, let us identify the dominant contribution to $\mathcal{F}(k, f_{\rm NL}^{\rm X})$ in the limit $k \ll 1$. Setting $\mathcal{M}_R(\sqrt{\alpha},0) \approx \mathcal{M}_R(k_1,0)$ and expanding $P_\phi(\sqrt{\alpha})$ at second order in the ratio k/k_1, we arrive at

$$\mathcal{F}(k, f_{\rm NL}^{\rm loc}) \approx f_{\rm NL}^{\rm loc} \tag{28a}$$

$$\mathcal{F}(k, f_{\rm NL}^{\rm eq}) \approx f_{\rm NL}^{\rm eq}\left[3\Sigma_R\left(\frac{2(n_s-4)}{3}\right)k^{\frac{2(4-n_s)}{3}} + \frac{1}{2}(n_s-4)\Sigma_R(-2)k^2\right]\sigma^{-2} \tag{28b}$$

$$\mathcal{F}(k, f_{\rm NL}^{\rm fol}) \approx \frac{3}{2}f_{\rm NL}^{\rm fol}\Sigma_R\left(\frac{n_s-4}{3}\right)k^{\frac{4-n_s}{3}}\sigma^{-2} , \tag{28c}$$

assuming no running scalar index, i.e. $dn_s/d\ln k = 0$. The auxiliary function $\Sigma_R(n)$ is defined as

$$\Sigma_R(n) = \frac{1}{2\pi^2}\int_0^\infty dk\, k^{(2+n)}\mathcal{M}_R(k,0)^2 P_\phi(k) . \tag{29}$$

Hence, we have $\Sigma_R(0) \equiv \sigma^2$. For a nearly scale-invariant spectrum $n_s \approx 1$, we obtain $\mathcal{F}(k, f_{\rm NL}^{\rm fol}) \propto k$ and $\mathcal{F}(k, f_{\rm NL}^{\rm eq}) \propto k^2$, such that the non-Gaussian bias is $\Delta b_\kappa \propto k^{-1}$ and $\Delta b_\kappa =$const. for the folded and equilateral bispectrum, respectively. Therefore, at large scales, the scale-dependence of the non-Gaussian bias is much smaller for the folded template, and nearly absent for the equilateral shape. This make them much more difficult to detect with galaxy surveys [152]. However, the equilateral and folded non-Gaussian bias depend sensitively upon the mass scale M through the multiplicative factor σ^{-2}. For example, choosing $R = 5\ h^{-1}$Mpc instead of $R = 1\ h^{-1}$Mpc would increase the effect by a factor of ~ 3. In the high peak limit, $\sigma^{-2} \approx b_{\rm L}/\delta_{\rm c}(z)$, which cancels out the dependence on redshift but enhances the sensitivity to the halo bias, i.e. $\Delta b_\kappa \propto b_{\rm L}^2$. By contrast, $\Delta b_\kappa \propto b_{\rm L}$ for the local $f_{\rm NL}^{\rm loc}$ model.

At this point, it is appropriate to mention a few caveats to these calculations. Firstly, Eq. (26) assumes that the tracers form after a spherical collapse, which may be a good approximation for the massive halos only. If one instead considers the ellipsoidal collapse dynamics, in which the evolution of a perturbation depends upon the three eigenvalues of the initial tidal shear, $\delta_{\rm c}(0)$ should be replaced by its ellipsoidal counterparts $\delta_{\rm ec}(0)$ which is always larger than the spherical value [108]. In this model, the scale-dependent bias Δb_κ is thus enhanced by a factor $\delta_{\rm ec}(0)/\delta_{\rm c}(0)$ [149]. Secondly, Eq. (26) assumes that the biasing of the surveyed objects is described by the peak height ν only, or equivalently, the hosting halo mass M. However, this may not be true

for quasars whose activity may be triggered by merger of halos [153, 154]. Reference [148] used the EPS formalism to estimate the bias correction Δb_merger induced by recent mergers,

$$\Delta b_\mathrm{merger} = \delta_\mathrm{c}^{-1} \ , \tag{30}$$

so the factor $b_1(M) - 1$ should be replaced by $b_1(M) - 1 - \delta_\mathrm{c}^{-1} \approx b_1(M) - 1.6$. The validity of this result should be evaluated with cosmological simulations of quasars formation. In this respect, semi-analytic models of galaxy formation suggest that merger-triggered objects such as quasars do not cluster much differently than other tracers of the same mass [155]. However, this does not mean that the same should hold for the non-gaussian scale dependent bias. Still, since the recent merger model is an extreme case it seems likely that the actual bias correction is $0 < \Delta b_\mathrm{merger} < \delta_\mathrm{c}^{-1}$. Thirdly, the scale-dependent bias has been derived using the Newtonian approximation to the Poisson equation, so one may wonder whether general relativistic (GR) corrections to $\mathcal{M}_R(k)^{-1}$ suppress the effect on scales comparable to the Hubble radius. Reference [156] showed how large scale primordial NG induced by GR corrections propagates onto small scales once cosmological perturbations reenter the Hubble radius in the matter dominated era. This effect generates a scale-dependent bias comparable, albeit of opposite sign to that induced by local NG [152]. However, this issue deserves further clarification as [157] have recently argued that there are no GR corrections to the non-Gaussian bias and that the scaling $\Delta b_\kappa \propto k^{-2}$ applies down to the smallest wavenumbers.

Finally, we can also ask ourselves whether higher-order terms in the series expansion (25) furnish corrections to the non-Gaussian bias of magnitude comparable to Eq.(24). In the $f_\mathrm{NL}^\mathrm{loc}$ model, the power spectrum of biased tracers of the density field can also be obtained from a local Taylor series in the evolved (Eulerian) density contrast δ and the Gaussian part ϕ of the initial (Lagrangian) curvature perturbation [158, 67]. Using this approach, it can be shown that the halo power spectrum arising from the first order terms of the local bias expansion can be cast into the form [158]

$$P_\mathrm{h}(k) = \left[b_1(M) + f_\mathrm{NL}^\mathrm{loc} b_\phi(k) \right]^2 P_R(k) \tag{31}$$

Hence, we obtain a second order term proportional to $(f_\mathrm{NL}^\mathrm{loc})^2 \mathcal{M}_R^{-2} P_R(k) = (f_\mathrm{NL}^\mathrm{loc})^2 P_\phi(k)$ which, however, contributes only at very small wavenumber $k \lesssim 0.001 \ h^{-1}\mathrm{Mpc}$. There is another second order correction to the halo power spectrum that reads [100]

$$\Delta P_\mathrm{h}(k) = \frac{4}{3} (f_\mathrm{NL}^\mathrm{loc})^2 \left[b_1(M) - 1 \right]^2 \delta_\mathrm{c}^2(z) \, S_3^{(1)}(M) \mathcal{M}_R(k,0) P_\phi(k) \ . \tag{32}$$

Its magnitude relative to the term linear in $f_\mathrm{NL}^\mathrm{loc}$, Eq.(24), is approximately 0.03 at redshift $z = 1.8$ and for a halo mass $M = 10^{13} \ \mathrm{M}_\odot/h$. Although this contribution becomes increasingly important at higher redshift, it is fairly small for realistic values of $f_\mathrm{NL}^\mathrm{loc}$. All this suggests that Eq. (24) is the dominant contribution to the non-Gaussian bias in the wavenumber range $0.001 \lesssim k \lesssim 0.1 \ h\mathrm{Mpc}^{-1}$.

4.3.2. Comparison with simulations In order to fully exploit the potential of forthcoming large scale surveys, a number of studies have tested the theoretical prediction Eq.(24) against the outcome of large numerical simulations [13, 42, 43, 98, 44, 67].

At the lowest order, there are two additional albeit relatively smaller corrections to the Gaussian bias which arise from the dependence of both the halo number density

$n(M, z)$ and the matter power spectrum $P_\delta(k, z)$ on primordial NG [42]. Firstly, assuming the peak-background split holds, the change in the mean number density of halos induces a scale-independent offset which we denote $\Delta b_{\rm I}(f_{\rm NL}^{\rm loc})$. In terms of the non-Gaussian fractional correction $R(\nu, f_{\rm NL}^{\rm loc})$ to the mass function, this contribution is

$$\Delta b_{\rm I}(f_{\rm NL}^{\rm loc}) = -\frac{1}{\sigma} \frac{\partial}{\partial \nu} \ln\left[R(\nu, f_{\rm NL}^{\rm loc}) \right] . \tag{33}$$

It is worth noticing that $\Delta b_{\rm I}(f_{\rm NL}^{\rm loc})$ has a sign opposite to that of $f_{\rm NL}^{\rm loc}$, because the bias decreases when the mass function goes up. Secondly, we also need to account for the change in the matter power spectrum (see §3). As a result, non-Gaussianity of the $f_{\rm NL}^{\rm loc}$ type adds a correction $\Delta b(k, f_{\rm NL}^{\rm loc})$ to the bias $b(k)$ of dark matter halos that reads [42]

$$\Delta b(k, f_{\rm NL}^{\rm loc}) = \Delta b_\kappa(k, f_{\rm NL}^{\rm loc}) + \Delta b_{\rm I}(f_{\rm NL}^{\rm loc}) + b_1(M) \left(\frac{P_\delta(k, f_{\rm NL}^{\rm loc})}{P_\delta(k, 0)} - 1 \right) \tag{34}$$

at first order in $f_{\rm NL}^{\rm loc}$. The linear bias b_1 needs to be measured accurately as it controls the strength of the scale-dependent bias correction Δb_κ. In this respect, the ratio $P_{\rm h\delta}(k)/P_\delta(k)$, where $P_{\rm h\delta}(k)$ is the halo-matter cross power spectrum, is a better proxy for the halo bias as it is less sensitive to shot-noise.

Reference [42] find that the inclusion of these extra terms substantially improves the comparison between the theory and the simulations. Considering only the scale-dependent shift Δb_κ leads to an apparent suppression of the effect in simulations relative to the theory. Including the scale-independent offset $\Delta b_{\rm I}$ considerably improves the agreement at all scales. Finally, adding the scale-dependent term $b_1(M)(P_{\rm mm}(k, f_{\rm NL}^{\rm loc})/P_{\rm mm}(k, 0) - 1)$ further adjusts the match at small scale $k \gtrsim 0.05$ $h{\rm Mpc}^{-1}$ by making the non-Gaussian bias shift less negative. Taking into account second- and higher-order corrections could extend the validity of the theory up to scales $k \sim 0.1 - 0.3$ $h{\rm Mpc}^{-1}$ [67].

Auto- and cross-power analyses may not agree with each other if the halos and dark matter do not trace each other on scale $k \lesssim 0.01$ $h{\rm Mpc}^{-1}$ where the non-Gaussian bias is large, i.e. if there is stochasticity. Fig.2 shows $P_{\rm h\delta}(k)$ and $P_{\rm h}(k)$ averaged over 8 realisations of the models with $f_{\rm NL}^{\rm loc} = 0, \pm 100$. The same Gaussian random seed field ϕ was used in each set of runs so as to minimize the sampling variance. Measurements of the non-Gaussian bias correction obtained with the halo-halo or the halo-matter power spectrum are in a good agreement with each other, indicating that non-Gaussianity does not induce stochasticity and the predicted scaling Eq.(24) applies equally well for the auto- and cross-power spectrum. However, while a number of numerical studies of the $f_{\rm NL}^{\rm loc}$ model have confirmed the scaling $\Delta b_\kappa(k, f_{\rm NL}^{\rm loc}) \propto \mathcal{M}_R(k)^{-1}$ and the redshift dependence $\propto D(z)^{-1}$ [13, 42, 43, 98], the exact amplitude of the non-Gaussian bias correction remains somewhat debatable. Reference [42], who use SO halos and include the scale-independent offset $\Delta b_{\rm I}$, find satisfactory agreement with the theory. By contrast, [98, 43], who use FOF halos, find that Eq.(24) is a good fit to the simulations only upon replacing δ_c by $q\delta_c$ with $q \simeq 0.75$. Part of the discrepancy may be due to the fact that [98, 43] do not include $\Delta b_{\rm I}$, which leads to an apparent suppression of the effect. Another possible source of discrepancy may be choice of the halo finder. In this regards, Fig. 3 shows the non-Gaussian bias correction obtained with FOF halos. The best-fit values of $f_{\rm NL}^{\rm loc}$ are somewhat below the input values of ± 100, in agreement with the findings of [98, 43]. This indicates that the choice of halo finder also affects the magnitude of the non-Gaussian halo bias. Discrepancies have also been observed
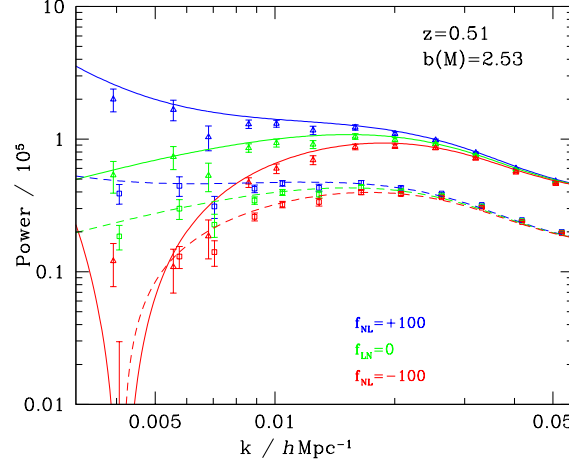
Figure 2. Halo-halo and halo-matter power spectra $P_{\rm h}(k)$ and $P_{\rm h\delta}(k)$ measured in simulations of the Gaussian model and of the local $f_{\rm NL}^{\rm loc}$ type with $f_{\rm NL}^{\rm loc} = \pm 100$. Halos of mass $M > 2 \times 10^{13}$ $M_\odot/h$ were identified at redshift $z = 2$ with a SO finder. The linear Gaussian bias of this sample is $b_1(M) = 2.53$. The error bars represent the scatter among 8 realizations. The solid and dashed curve show the theoretical $P_{\rm h}(k)$ and $P_{\rm h\delta}(k)$ obtained wih the non-Gaussian bias correction Eq.(34). For $f_{\rm NL}^{\rm loc} = -100$, the cross-power spectrum is negative on scales $k \lesssim 0.005$ $h{\rm Mpc}^{-1}$, in good agreement with the theoretical prediction.

between the theoretical and measured non-Gaussian bias corrections in non-Gaussian models of the local cubic-order coupling $g_{\rm NL}^{\rm loc}\phi^3$ [100]. Understanding these results will clearly require a better theoretical modeling of halo clustering.

4.3.3. Redshift distortions   Peculiar velocities generate systematic differences between the spatial distribution of data in real and redshift space. These redshift distortions must be properly taken into account in order to extract $f_{\rm NL}^{\rm X}$ from redshift surveys. On the linear scales of interest, the redshift space power spectrum of biased tracers reads as [159, 160]

$$P^s(k,\mu) = \left[b_1^2 P_\delta(k) + 2b_1 f \mu^2 P_{\delta\theta}(k) + f^2 \mu^4 P_\theta(k)\right] , \tag{35}$$

where $P_{\delta\theta}$ and P_θ are the density-velocity and velocity divergence power spectra, μ is the cosine of the angle between the wavemode $\mathbf{k}$ and the line of sight and f is the logarithmic derivative of the growth factor. For P_θ, the 1-loop correction due to primordial NG is identical to Eq.(13) provided $F_2(\mathbf{k}_1, \mathbf{k}_2)$ is replaced by the kernel $G_2(\mathbf{k}_1, \mathbf{k}_2) = 3/7 + \mu(k_1/k_2 + k_2/k_1)/2 + 4\mu^2/7$ describing the 2nd order evolution of the velocity divergence [58]. For $P_{\delta\theta}$, this correction is

$$\Delta P_{\delta\theta}^{\rm NG}(k) = \int \frac{d^3\mathbf{q}}{(2\pi)^3} \left[F_2(\mathbf{q}, \mathbf{k} - \mathbf{q}) + G_2(\mathbf{q}, \mathbf{k} - \mathbf{q})\right] B_0(-\mathbf{k}, \mathbf{q}, \mathbf{k} - \mathbf{q}) . \tag{36}$$

Again, causality implies that $G_2(\mathbf{k}_1, \mathbf{k}_2)$ vanishes in the limit $\mathbf{k}_1 = -\mathbf{k}_2$. For unbiased tracers with $b_1 = 1$, the linear Kaiser relation is thus recovered at large scales $k \lesssim 0.01$ $h{\rm Mpc}^{-1}$ (see also [61]). For biased tracers, we still expect the Kaiser formula to be valid, but the distortion parameter β should now be equal to
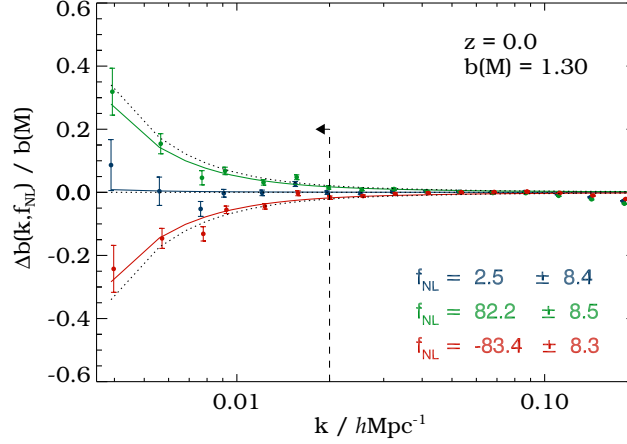
Figure 3. Fractional correction to the Gaussian halo bias in the $f_{\rm NL}^{\rm loc} = \pm 100$ and Gaussian models. In constrast to Fig. 2, halos were identified with a FOF finder of linking length $b = 0.2$. Only the wavemodes to the left of the vertical line were used to fit $\Delta b_\kappa(k, f_{\rm NL}^{\rm loc})$. The best-fit value of $f_{\rm NL}^{\rm loc}$ and the corresponding 1σ error is quoted for each model (Figure taken from [166]).

$\beta = f/(b_1 + \Delta b_\kappa)$, where $\Delta b_\kappa(k, f_{\rm NL}^{\rm X})$ is the scale-dependent bias induced by the primordial non-Gaussianity.

4.3.4. Mitigating cosmic variance and shot-noise Because of the finite number of large scale wavemodes accessible to a survey, any large scale measurement of the power spectrum is limited by the cosmic (or sampling) variance caused by the random nature of the wavemodes. For discrete tracers such as galaxies, the shot noise is another source of error. For weak primordial NG, the relative error on the power spectrum P is $\sigma_P/P \approx 1/\sqrt{N}(1 + \sigma_n^2/P)$, where N is the number of independent modes measured and σ_n^2 is the shot-noise [161]. Under the standard assumption of Poisson sampling, σ_n^2 equals the inverse of the number density $1/\bar{n}$ and causes a scale-independent enhancement of the power spectrum. The extent to which one can improve the observational limits on the nonlinear will strongly depend on our ability to minimize the impact of these two sources of errors. By comparing differently biased tracers of the same surveyed volume [162, 163] and suitably weighting galaxies (by the mass of their host halo for instance) [164, 165], it should be possible to circumvent these problems and considerably improve the detection level.

Figure 3 illustrates how the impact of sampling variance on the measurement of $f_{\rm NL}^{\rm loc}$ can be mitigated. Namely, the data points show the result of taking the ratio $P_{\rm h}(k, f_{\rm NL}^{\rm loc})/P_\delta(k, f_{\rm NL}^{\rm loc})$ for each set of runs with same Gaussian random seed field ϕ before averaging over the realisations. This procedure is equivalent to the multi-tracers method advocated by [162]. Here, P_δ can be thought as mimicking the power spectrum of a nearly unbiased tracer of the mass density field with high number density. Although, in practical applications, using the dark matter field works better [166], in real data P_δ should be replaced by a tracer of the same surveyed volume different than the one used to compute $P_{\rm h}$. Figure 3 also shows that, upon taking out most of the cosmic variance, there is some residual noise caused by the discrete

nature of the dark matter halos. As shown recently [165] however, weighting the halos according to their mass can dramatically reduce the shot noise relative to the Poisson expectation, at least when compared against the dark matter. Applying such a weighting may thus significantly improve the error on the nonlinear parameter $f_{\rm NL}^{\rm loc}$, but this should be explored in realistic simulations of galaxies, especially because the halo mass M may not be easily measurable from real data [166]. This approach undoubtedly deserves further attention as it has the potential to substantially improve the extraction of the primordial non-Gaussian signal from galaxy surveys.

To conclude this Section, we note that, while the PDF of power values $P(\mathbf{k})$ has little discriminatory power (for large surveyed volume, it converges towards the Rayleigh distribution as a consequence of the central limit theorem) [167], the covariance of power spectrum measurements (which is sensitive to the selection function, but also to correlations among the phase of the Fourier modes) may provide quantitative limits on certain type of non-Gaussian models [161, 168].

4.4. Galaxy bispectrum and higher order statistics

Higher statistics of biased tracers, such as the galaxy bispectrum, are of great interest as they are much more sensitive to the shape of the primordial 3-point function than the power spectrum [12, 169, 170, 64, 44]. Therefore, they could break some of the degeneracies affecting the non-Gaussian halo bias (For example, the leading order scale-dependent correction to the Gaussian bias induced by the local quadratic and cubic coupling are fully degenerate [100]).

4.4.1. Normalized cumulants of the galaxy distribution
The skewness of the galaxy count probability distribution function could provide constraints on the amount of non-Gaussianity in the initial conditions. As discussed in §3 however, it is difficult to disentangle the primordial and gravitational causes of skewness in low redshift data unless the initial density field is strongly non-Gaussian. The first analyzes of galaxy catalogs in terms of count-in-cells densities all reached the conclusion that the skewness (and higher-order moments) of the observed galaxy count PDF is consistent with the value induced by gravitational instabilities of initially Gaussian fluctuations [50, 171, 172, 173, 54, 174]. Back then however, most of the galaxy samples available were not large enough to accurately determine the cumulants S_J at large scales [175]. Despite the 2 orders of magnitude increase in surveyed volume, these measurements are still sensitive to cosmic variance, i.e. to the presence of massive super-clusters or large voids. Nevertheless, the best estimates of the first normalized cumulants S_J of the galaxy PDF strongly suggest that high order galaxy correlation functions follow the hierarchical scaling predicted by the gravitational clustering of Gaussian ICs [176]. There is no evidence for strong non-Gaussianity in the initial density field as might by seeded by cosmic strings or textures [177].

The genus statistics of constant density surfaces through the galaxy distribution measures the relative abundance of low and high density regions as a function of the smoothing scale R and, therefore, could also be used as a diagnostic tool for primordial non-Gaussianity. While for a Gaussian random field the genus curve (i.e. the genus number as a function of the density contrast) is symmetric about $\delta_R = 0$ regardless the value of R, primordial NG and nonlinear gravitational evolution can disrupt this symmetry [178]. The effect of non-Gaussian ICs on the topology of the galaxy distribution has been explored in a number of papers [36, 179, 180, 181, 182].

For large values of R and a realistic amount of primordial NG, the genus statistics can also be expanded in a series whose coefficients are the normalized cumulants S_J of the smoothed galaxy density field. Therefore, the genus statistics essentially provides another measurement of the (large scale) cumulants of the galaxy distribution [183, 184].

4.4.2. Galaxy bispectrum Most of the scale-dependence of the primordial n-point functions is integrated out in the normalized cumulants, which makes them weakly sensitive to primordial NG. However, while the effect of non-Gaussian initial conditions, galaxy bias, gravitational instabilities etc. are strongly degenerated in the S_J, they imprint distinct signatures in the galaxy bispectrum $B_{\rm h}(\mathbf{k}_1, \mathbf{k}_2, \mathbf{k}_3)$, an accurate measurement of which could thus constrain the shape of the primordial 3-point function.

In the original derivation of [169], the large scale (unfiltered) galaxy bispectrum in the $f_{\rm NL}^{\rm loc}$ model is given by

$$B_{\rm h}(\mathbf{k}_1, \mathbf{k}_2, \mathbf{k}_3) = b_1^3 B_0(\mathbf{k}_1, \mathbf{k}_2, \mathbf{k}_3) + b_1^2 b_2 \Big[P_0(k_1) P_0(k_2) + (\text{cyc.}) \Big]$$
$$+ 2b_1^3 \Big[F_2(\mathbf{k}_1, \mathbf{k}_2) P_0(k_1) P_0(k_2) + (\text{cyc.}) \Big] . \tag{37}$$

Here, b_1 and b_2 are the first- and second-order bias parameters that describe galaxy biasing relation assumed local and deterministic [185]. The first term in the right-hand side is the primordial contribution which, for equilateral configurations and in the $f_{\rm NL}^{\rm loc}$ model, scales as $\mathcal{M}_R(k,z)^{-1}$ like in the matter bispectrum, Eq.(14). The two last terms are the contribution from nonlinear bias and the tree-level correction from gravitational instabilities, respectively. They have the smallest signal in squeezed configurations.

As recognized by [170, 64], Eq.(37) misses an important term that may significantly enhance the sensitivity of the galaxy bispectrum to non-Gaussian initial conditions. This contribution is sourced by the trispectrum $T_R(\mathbf{k}_1, \mathbf{k}_2, \mathbf{k}_3, \mathbf{k}_4)$ of the smoothed mass density field,

$$\frac{1}{2} b_1^2 b_2 \int \frac{d^3q}{(2\pi)^3} \, T_R(\mathbf{k}_1, \mathbf{k}_2, \mathbf{q}, \mathbf{k}_3 - \mathbf{q}) + (2 \text{ perms.}) , \tag{38}$$

and reduces at large scales to the sum of the linearly evolved primordial trispectrum $T_0(\mathbf{k}_1, \mathbf{k}_2, \mathbf{k}_3, \mathbf{k}_4)$ and a coupling between the primordial bispectrum $B_0(\mathbf{k}_1, \mathbf{k}_2, \mathbf{k}_3)$ (linear in $f_{\rm NL}^{\rm X}$) and the second order PT corrections (through the kernel $F_2(\mathbf{k}_1, \mathbf{k}_2)$). In the case of local non-Gaussianity and for equilateral configurations, the first piece proportional to T_0 scales as $(f_{\rm NL}^{\rm loc})^2 k^{-4}$ times the Gaussian tree-level prediction, with the same redshift dependence. Hence, it is similar to the second order correction $(f_{\rm NL}^{\rm loc})^2 \mathcal{M}_R^{-2} P_R(k)$ that appears in the halo power spectrum (see Eq.31). The second piece linear in $f_{\rm NL}^{\rm X}$ generates a signal at large scales for essentially all triangle shapes in the local model as well as in the case of equilateral NG. This second contribution is maximized in the squeezed limit (where it is one order of magnitude larger than the result obtained by [169]) which helps disentangling it from the Gaussian terms. Note that a strong dependence on triangle shape is also present in other NG scenarios such as the χ^2 model [58].

This newly derived contributions are claimed to lead to more than one order of magnitude improvement in certain limits [170], but it is not yet clear whether these gains can be realized in any realistic survey. To accurately predict the constraints that
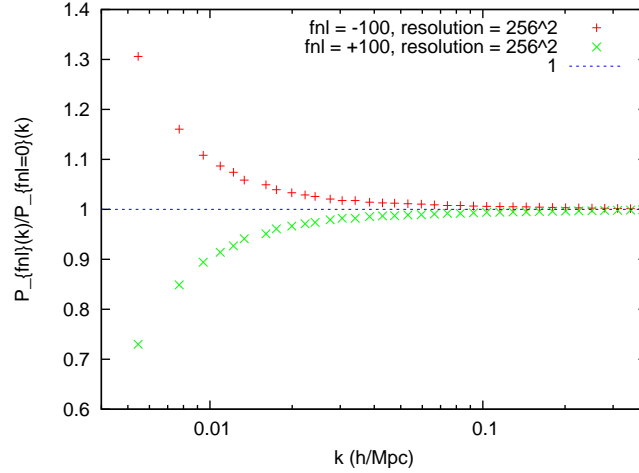
Figure 4. Ratio between the Lyman-α 3D flux power spectrum extracted from simulations of Gaussian and non-Gaussian initial conditions at redshift $z = 2$. The mean transmission is set to $\bar{F} = 0.8$ (Figure taken from [190]).

could be achieved with future measurements of the galaxy bispectrum, a comparison of these predictions with the halo bispectrum extracted from numerical simulations is highly desirable. To date, the only numerical study [44] has measured the halo bispectrum for some isosceles triangles ($k_1 = k_2$). While the shape dependence is in reasonable agreement with the theory, the observed k-dependence appears to depart from the predicted scaling.

4.5. Intergalactic medium and the Lyα forest

Primordial non-Gaussianity also affects the intergalactic medium (IGM) as a positive $f_{\mathrm{NL}}^{\mathrm{X}}$ enhances the formation of high-mass halos at early times and, therefore, accelerate reionization [186, 187, 188]. At lower redshift, small box hydrodynamical simulations of the Lyα forest indicate that non-Gaussian initial conditions could leave a detectable signature in the Lyα flux PDF, power spectrum and bispectrum [189]. However, while differences appear quite pronounced in the high transmissivity tail of the flux PDF (i.e. in underdense regions), the Lyα 1D flux power spectrum seems little affected. Given the small box size of these hydrodynamical simulations, it is worth exploring the effect in large N-body cosmological simulations using a semi-analytic modeling of the Lyα forest [190]. Figure 4 shows the imprint of local type NG on the Lyα 3D flux power spectrum (which is not affected by projection effects) extracted from a series of large simulations at $z = 2$. The Lyα transmitted flux is calculated in the Gunn-Peterson approximation [191]. A clear signature similar to the non-Gaussian halo bias can be seen and, as expected, it is of opposite sign since the Lyα forest is anti-biased relative to the mass density field (overdensities are mapped onto relatively low flux transmission). A detection of this effect, although challenging in particular because of continuum uncertainties, could be feasible with future data sets. The Lyα could thus provide interesting information on the non-Gaussian signal over a range of scale and redshift not easily accessible to galaxy and CMB observations [189, 190].

5. Current limits and prospects

As the importance of primordial non-Gaussianity relative to the non-Gaussianity induced by gravitational clustering and galaxy bias increases towards high redshift, the optimal strategy to constrain the nonlinear coupling parameter(s) with LSS is to use large scale, high-redshift observations [34].

5.1. Existing constraints on primordial NG

The non-Gaussian halo bias presently is the only LSS method that provides a robust limit on the magnitude of a primordial 3-point function of the local shape. It is a broadband effect that can be easily measured with photometric redshifts. The authors of [148] have applied Eq.(24) to constrain the value of $f_{\rm NL}^{\rm loc}$ using a compilation of large-scale clustering data. Their constraint arise mostly from the QSO sample at median redshift $z = 1.8$, which covers a large comoving volume and is highly biased, $b_1 = 2.7$. They obtain

$$-29 < f_{\rm NL}^{\rm loc} < +69 \tag{39}$$

at 95% confidence level. These limits are competitive with those from CMB measurements, $-10 < f_{\rm NL}^{\rm loc} < +74$ [192]. It is straightforward to translate this 2-σ limit into a constraint on the cubic order coupling $g_{\rm NL}^{\rm loc}$ since the non-Gaussian scale-dependent bias $\Delta b_\kappa(k, g_{\rm NL}^{\rm loc})$ has the same functional form as $\Delta b_\kappa(k, f_{\rm NL}^{\rm loc})$ [100]. Assuming $f_{\rm NL}^{\rm loc} = 0$, one obtains

$$-3.5 \times 10^5 < g_{\rm NL}^{\rm loc} < +8.2 \times 10^5 . \tag{40}$$

These limits are comparable with those inferred from an analysis of CMB data using n-point distribution functions, $-5.6 \times 10^5 < g_{\rm NL}^{\rm loc} < 6.4 \times 10^5$ [193].

Measurements of the galaxy bispectrum in several redshift catalogs have shown evidence for a configuration shape dependence in agreement with that predicted from gravitational instability, ruling out χ^2 initial conditions at the 95% C.L. [194, 195]. Recent analyses of the SDSS LRGs catalogue indicate that the shape dependence of the reduced 3-point correlation $Q_3 \sim \xi_3/(\xi_2)^2$ is also consistent with Gaussian ICs [196], although a primordial (hierarchical) non-Gaussian contribution in the range $Q_3 \sim 0.5 - 3$ cannot be ruled out [197]. Other LSS probes of primordial non-Gaussianity, such as the abundance of massive clusters, are still too affected by systematics to furnish tight constraints on the shape and magnitude of a primordial 3-point function, although the observation of a handful of unexpectedly massive high-redshift clusters has been interpreted as evidence of a substantial degree of primordial NG [198, 199, 200].

5.2. Future prospects

Improving the current limits will further constrain the physical mechanisms for the generation of cosmological perturbations.

The non-Gaussian halo bias also leaves a signature in cross-correlation statistics of weak cosmic shear (galaxy-galaxy and galaxy-CMB) [201, 202] and in the integrated Sachs-Wolfe (ISW) effect [148, 149]. Measurements of the lensing bispectrum could also constrain a number of non-Gaussian models [203]. However, galaxy clustering will undoubtedly offer the most promising LSS diagnostic of primordial non-Gaussianity. The detectability of a local primordial bispectrum has been assessed in a series of

papers. It is expected that future all-sky galaxy surveys will achieve constraints of the order of $\Delta f_{\mathrm{NL}}^{\mathrm{loc}} \sim 1$ assuming all systematics are reasonably under control [95, 148, 149, 158, 137, 204, 205, 206]. Realistic models of cubic type non-Gaussianity [100], modifications of the initial vacuum state or horizon-scale GR corrections [152] should also be tested with future measurement of the galaxy power spectrum.

Upcoming observations of high redshift clusters will provide increased leverage on measurement of primordial non-Gaussianity with abundances and possibly put limits on any nonlinear parameter $f_{\mathrm{NL}}^{\mathrm{X}}$ at the level of a few tens [127]. Combining the information provided by the evolution of the mass function and power spectrum of galaxy clusters can yield constraints with a precision $\Delta f_{\mathrm{NL}}^{\mathrm{loc}} \sim 10$ for a wide field survey covering half of the sky [200]. Alternatively, using the full covariance of cluster counts (which is sensitive to the non-Gaussian halo bias) can furnish constraints of $\Delta f_{\mathrm{NL}}^{\mathrm{loc}} \sim 1 - 5$ for a Dark Energy Survey-type experiment [207, 208].

As emphasized in §4 however, the exact magnitude of the non-Gaussian halo bias is still uncertain at the $\sim 20\%$ level, partly due to the freedom at the definition of the halo mass. Understanding this type of systematics will be crucial to set reliable constraints on a primordial non-Gaussian component. To fully exploit the potential of future galaxy surveys, it will also be essential to extend the theoretical and numerical analyses to other bispectrum shapes than the local template used so far. Ultimately, the gain that can be achieved will critically depend on our ability to minimize the impact of sampling variance and shot-noise. In this regards, multi-tracers methods combined with optimal weighting schemes should deserve further attention as they hold the promise to become the most accurate method to extract the primordial non-Gaussian signal from galaxy surveys [162, 164, 163, 165].

6. Acknowledgments

[1] V. F. Mukhanov and G. V. Chibisov. Quantum fluctuations and a nonsingular universe. *Soviet Journal of Experimental and Theoretical Physics Letters*, 33:532–+, May 1981.

[2] A. A. Starobinsky. Dynamics of phase transition in the new inflationary universe scenario and generation of perturbations. *Physics Letters B*, 117:175–178, November 1982.

[3] S. W. Hawking. The development of irregularities in a single bubble inflationary universe. *Physics Letters B*, 115:295–297, September 1982.

[4] A. H. Guth and S.-Y. Pi. Fluctuations in the new inflationary universe. *Physical Review Letters*, 49:1110–1113, October 1982.

[5] T. J. Allen, B. Grinstein, and M. B. Wise. Non-gaussian density perturbations in inflationary cosmologies. *Physics Letters B*, 197:66–70, October 1987.

[6] T. Falk, R. Rangarajan, and M. Srednicki. Dependence of density perturbations on the coupling constant in a simple model of inflation. *Phys. Rev. D.* , 46:4232–4234, November 1992.

[7] A. Gangui, F. Lucchin, S. Matarrese, and S. Mollerach. The three-point correlation function of the cosmic microwave background in inflationary models. *Astrophys. J.* , 430:447–457, August 1994.

[8] E. Komatsu, J. Dunkley, M. R. Nolta, C. L. Bennett, B. Gold, G. Hinshaw, N. Jarosik, D. Larson, M. Limon, L. Page, D. N. Spergel, M. Halpern, R. S. Hill, A. Kogut, S. S. Meyer,

G. S. Tucker, J. L. Weiland, E. Wollack, and E. L. Wright. Five-Year Wilkinson Microwave Anisotropy Probe Observations: Cosmological Interpretation. *Astrophys. J. Suppl.* , 180:330–376, February 2009.

[9] U. Seljak and M. Zaldarriaga. Signature of Gravity Waves in the Polarization of the Microwave Background. *Physical Review Letters*, 78:2054–2057, March 1997.

[10] M. Kamionkowski, A. Kosowsky, and A. Stebbins. A Probe of Primordial Gravity Waves and Vorticity. *Physical Review Letters*, 78:2058–2061, March 1997.

[11] L. Verde, L. Wang, A. F. Heavens, and M. Kamionkowski. Large-scale structure, the cosmic microwave background and primordial non-Gaussianity. *Mon. Not. R. Astron. Soc.* , 313:141–147, March 2000.

[12] R. Scoccimarro, E. Sefusatti, and M. Zaldarriaga. Probing primordial non-Gaussianity with large-scale structure. *Phys. Rev. D.* , 69(10):103513–+, May 2004.

[13] N. Dalal, O. Doré, D. Huterer, and A. Shirokov. Imprints of primordial non-Gaussianities on large-scale structure: Scale-dependent bias and abundance of virialized objects. *Phys. Rev. D.* , 77(12):123514–+, June 2008.

[14] D. S. Salopek and J. R. Bond. Nonlinear evolution of long-wavelength metric fluctuations in inflationary models. *Phys. Rev. D.* , 42:3936–3962, December 1990.

[15] J. Maldacena. Non-gaussian features of primordial fluctuations in single field inflationary models. *Journal of High Energy Physics*, 5:13–+, May 2003.

[16] V. Acquaviva, N. Bartolo, S. Matarrese, and A. Riotto. Gauge-invariant second-order perturbations and non-Gaussianity from inflation. *Nuclear Physics B*, 667:119–148, September 2003.

[17] P. Creminelli and M. Zaldarriaga. A single-field consistency relation for the three-point function. *Journal of Cosmology and Astro-Particle Physics*, 10:6–+, October 2004.

[18] A. Linde and V. Mukhanov. Non-Gaussian isocurvature perturbations from inflation. *Phys. Rev. D.* , 56:535–+, July 1997.

[19] D. H. Lyth, C. Ungarelli, and D. Wands. Primordial density perturbation in the curvaton scenario. *Phys. Rev. D.* , 67(2):023503–+, January 2003.

[20] T. Falk, R. Rangarajan, and M. Srednicki. The angular dependence of the three-point correlation function of the cosmic microwave background radiation as predicted by inflationary cosmologies. *Astrophys. J. Lett.* , 403:L1–L3, January 1993.

[21] J. Lesgourgues, D. Polarski, and A. A. Starobinsky. Quantum-to-classical transition of cosmological perturbations for non-vacuum initial states. *Nuclear Physics B*, 497:479–508, February 1997.

[22] G. Dvali, A. Gruzinov, and M. Zaldarriaga. Cosmological perturbations from inhomogeneous reheating, freeze-out, and mass domination. *Phys. Rev. D.* , 69(8):083505–+, April 2004.

[23] J.-L. Lehners and P. J. Steinhardt. Non-Gaussian density fluctuations from entropically generated curvature perturbations in ekpyrotic models. *Phys. Rev. D.* , 77(6):063533–+, March 2008.

[24] D. Babich, P. Creminelli, and M. Zaldarriaga. The shape of non-Gaussianities. *Journal of Cosmology and Astro-Particle Physics*, 8:9–+, August 2004.

[25] J. R. Fergusson and E. P. S. Shellard. Shape of primordial non-Gaussianity and the CMB bispectrum. *Phys. Rev. D.* , 80(4):043510–+, August 2009.

[26] E. Komatsu and D. N. Spergel. Acoustic signatures in the primary microwave background bispectrum. *Phys. Rev. D.* , 63(6):063002–+, March 2001.

[27] P. Creminelli, A. Nicolis, L. Senatore, M. Tegmark, and M. Zaldarriaga. Limits on non-Gaussianities from WMAP data. *Journal of Cosmology and Astro-Particle Physics*, 5:4–+, May 2006.

[28] P. D. Meerburg, J. P. van der Schaar, and P. Stefano Corasaniti. Signatures of initial state modifications on bispectrum statistics. *Journal of Cosmology and Astro-Particle Physics*, 5:18–+, May 2009.

[29] F. Bernardeau, S. Colombi, E. Gaztañaga, and R. Scoccimarro. Large-scale structure of the Universe and cosmological perturbation theory. *Phys. Rep.* , 367:1–248, September 2002.

[30] J. E. Gunn and J. R. Gott, III. On the Infall of Matter Into Clusters of Galaxies and Some Effects on Their Evolution. *Astrophys. J.* , 176:1–+, August 1972.

[31] J. R. Bond and S. T. Myers. The Peak-Patch Picture of Cosmic Catalogs. I. Algorithms. *Astrophys. J. Suppl.* , 103:1–+, March 1996.

[32] R. Durrer. Topological defects in cosmology. *New Astronomy Review*, 43:111–156, July 1999.

[33] A. Vilenkin and E. P. S. Shellard. *Cosmic Strings and Other Topological Defects.* July 2000.

[34] L. Verde, R. Jimenez, M. Kamionkowski, and S. Matarrese. Tests for primordial non-Gaussianity. *Mon. Not. R. Astron. Soc.* , 325:412–418, July 2001.

[35] L. Moscardini, S. Matarrese, F. Lucchin, and A. Messina. Non-Gaussian initial conditions in cosmological N-body simulations. II - Cold Dark Matter models. *Mon. Not. R. Astron. Soc.* , 248:424–438, February 1991.

[36] D. H. Weinberg and S. Cole. Non-Gaussian fluctuations and the statistics of galaxy clustering. *Mon. Not. R. Astron. Soc.* , 259:652–694, December 1992.

[37] P. Coles, L. Moscardini, F. Lucchin, S. Matarrese, and A. Messina. Skewness as a Test of Non-Gaussian Primordial Density Fluctuations. *Mon. Not. R. Astron. Soc.* , 264:749–+, October 1993.

[38] E. Gaztanaga and P. Maehoenen. Large-Scale Clustering from Non-Gaussian Texture Models. *Astrophys. J. Lett.* , 462:L1+, May 1996.

[39] M. White. Higher order moments of the density field in a parametrized sequence of non-Gaussian theories. *Mon. Not. R. Astron. Soc.* , 310:511–516, December 1999.

[40] H. Mathis, J. Silk, L. M. Griffiths, and M. Kunz. Constraining cosmic microwave background consistent primordial voids with cluster evolution. *Mon. Not. R. Astron. Soc.* , 350:287–297, May 2004.

[41] M. Grossi, E. Branchini, K. Dolag, S. Matarrese, and L. Moscardini. The mass density field in simulated non-Gaussian scenarios. *Mon. Not. R. Astron. Soc.* , 390:438–446, October 2008.

[42] V. Desjacques, U. Seljak, and I. T. Iliev. Scale-dependent bias induced by local non-Gaussianity: a comparison to N-body simulations. *Mon. Not. R. Astron. Soc.*, 396:85–96, June 2009.

[43] A. Pillepich, C. Porciani, and O. Hahn. Halo mass function and scale-dependent bias from N-body simulations with non-Gaussian initial conditions. *Mon. Not. R. Astron. Soc.* , 402:191–206, February 2010.

[44] T. Nishimichi, A. Taruya, K. Koyama, and C. Sabiu. Scale Dependence of Halo Bispectrum from Non-Gaussian Initial Conditions in Cosmological N-body Simulations. *ArXiv e-prints*, November 2009.

[45] R. Vio, P. Andreani, and W. Wamsteker. Numerical Simulation of Non-Gaussian Random Fields with Prescribed Correlation Structure. *Pub. Astron. Soc. Pac.*, 113:1009–1020, August 2001.

[46] X. Luo and D. N. Schramm. Kurtosis, skewness, and non-Gaussian cosmological density perturbations. *Astrophys. J.* , 408:33–42, May 1993.

[47] E. L. Lokas, R. Juszkiewicz, D. H. Weinberg, and F. R. Bouchet. Kurtosis of large-scale cosmic fields. *Mon. Not. R. Astron. Soc.* , 274:730–744, June 1995.

[48] P. J. E. Peebles. *The large-scale structure of the universe.* 1980.

[49] J. N. Fry. The Galaxy correlation hierarchy in perturbation theory. *Astrophys. J.* , 279:499–510, April 1984.

[50] P. Coles and C. S. Frenk. Skewness and large-scale structure. *Mon. Not. R. Astron. Soc.* , 253:727–737, December 1991.

[51] F. R. Bouchet, R. Juszkiewicz, S. Colombi, and R. Pellat. Weakly nonlinear gravitational instability for arbitrary Omega. *Astrophys. J. Lett.* , 394:L5–L8, July 1992.

[52] R. Juszkiewicz, F. R. Bouchet, and S. Colombi. Skewness induced by gravity. *Astrophys. J. Lett.* , 412:L9–L12, July 1993.

[53] O. Lahav, M. Itoh, S. Inagaki, and Y. Suto. Non-Gaussian signatures from Gaussian initial fluctuations - Evolution of skewness and kurtosis from cosmological simulations in the highly nonlinear regime. *Astrophys. J.* , 402:387–397, January 1993.

[54] J. N. Fry and R. J. Scherrer. Skewness in large-scale structure and non-Gaussian initial conditions. *Astrophys. J.* , 429:36–42, July 1994.

[55] R. Juszkiewicz, D. H. Weinberg, P. Amsterdamski, M. Chodorowski, and F. Bouchet. Weakly nonlinear Gaussian fluctuations and the edgeworth expansion. *Astrophys. J.* , 442:39–56, March 1995.

[56] M. J. Chodorowski and F. R. Bouchet. Kurtosis in large-scale structure as a constraint on non-Gaussian initial conditions. *Mon. Not. R. Astron. Soc.* , 279:557–563, March 1996.

[57] E. Gaztanaga and P. Fosalba. Cosmological perturbation theory and the spherical collapse model - II. Non-Gaussian initial conditions. *Mon. Not. R. Astron. Soc.* , 301:524–534, December 1998.

[58] R. Scoccimarro. Gravitational Clustering from χ^2 Initial Conditions. *Astrophys. J.* , 542:1–8, October 2000.

[59] N. Turok and D. N. Spergel. Scaling solution for cosmological sigma models at large N. *Physical Review Letters*, 66:3093–3096, June 1991.

[60] R. Durrer, R. Juszkiewicz, M. Kunz, and J.-P. Uzan. Skewness as a probe of non-Gaussian

initial conditions. *Phys. Rev. D.* , 62(2):021301–+, July 2000.

[61] T. Y. Lam, V. Desjacques, and R. K. Sheth. The non-linear redshift space probability distribution function in models with local primordial non-Gaussianity. *Mon. Not. R. Astron. Soc.* , 402:2397–2402, March 2010.

[62] T. Y. Lam and R. K. Sheth. The non-linear probability distribution function in models with local primordial non-Gaussianity. *Mon. Not. R. Astron. Soc.* , 395:1743–1748, May 2009.

[63] A. Taruya, K. Koyama, and T. Matsubara. Signature of primordial non-Gaussianity on the matter power spectrum. *Phys. Rev. D.* , 78(12):123534–+, December 2008.

[64] E. Sefusatti. One-loop perturbative corrections to the matter and galaxy bispectrum with non-Gaussian initial conditions. *Phys. Rev. D.* , 80(12):123002–+, December 2009.

[65] M. H. Goroff, B. Grinstein, S.-J. Rey, and M. B. Wise. Coupling of modes of cosmological mass density fluctuations. *Astrophys. J.* , 311:6–14, December 1986.

[66] N. Makino, M. Sasaki, and Y. Suto. Analytic approach to the perturbative expansion of nonlinear gravitational fluctuations in cosmological density and velocity fields. *Phys. Rev. D.* , 46:585–602, July 1992.

[67] T. Giannantonio and C. Porciani. Structure formation from non-Gaussian initial conditions: multivariate biasing, statistics, and comparison with N-body simulations. *ArXiv e-prints*, November 2009.

[68] S. Matarrese and M. Pietroni. Resumming cosmic perturbations. *Journal of Cosmology and Astro-Particle Physics*, 6:26–+, June 2007.

[69] K. Izumi and J. Soda. Renormalized Newtonian cosmic evolution with primordial non-Gaussianity. *Phys. Rev. D.* , 76(8):083517–+, October 2007.

[70] N. Bartolo, J. P. Beltran Almeida, S. Matarrese, M. Pietroni, and A. Riotto. Signatures of Primordial non-Gaussianities in the Matter Power-Spectrum and Bispectrum: the Time-RG Approach. *ArXiv e-prints*, December 2009.

[71] P. Catelan and L. Moscardini. Kurtosis and large-scale structure. *Astrophys. J.* , 426:14–18, May 1994.

[72] L. Verde and A. F. Heavens. On the Trispectrum as a Gaussian Test for Cosmology. *Astrophys. J.* , 553:14–24, May 2001.

[73] E. Sefusatti, M. Crocce, and V. Desjacques. The Matter Bispectrum in N-body Simulations with non-Gaussian Initial Conditions. *ArXiv e-prints*, February 2010.

[74] A. Loeb and M. Zaldarriaga. Measuring the Small-Scale Power Spectrum of Cosmic Density Fluctuations through 21cm Tomography Prior to the Epoch of Structure Formation. *Physical Review Letters*, 92(21):211301–+, May 2004.

[75] A. Cooray. Large-scale non-Gaussianities in the 21-cm background anisotropies from the era of reionization. *Mon. Not. R. Astron. Soc.* , 363:1049–1056, November 2005.

[76] A. Pillepich, C. Porciani, and S. Matarrese. The Bispectrum of Redshifted 21 Centimeter Fluctuations from the Dark Ages. *Astrophys. J.* , 662:1–14, June 2007.

[77] M. Bartelmann and P. Schneider. Weak gravitational lensing. *Phys. Rep.* , 340:291–472, January 2001.

[78] S. D. M. White and M. J. Rees. Core condensation in heavy halos - A two-stage theory for galaxy formation and clustering. *Mon. Not. R. Astron. Soc.* , 183:341–358, May 1978.

[79] N. Kaiser. On the spatial correlations of Abell clusters. *Astrophys. J. Lett.* , 284:L9–L12, September 1984.

[80] V. Desjacques. Baryon acoustic signature in the clustering of density maxima. *Phys. Rev. D.* , 78(10):103503–+, November 2008.

[81] P. McDonald and A. Roy. Clustering of dark matter tracers: generalizing bias for the coming era of precision LSS. *Journal of Cosmology and Astro-Particle Physics*, 8:20–+, August 2009.

[82] C. Lacey and S. Cole. Merger Rates in Hierarchical Models of Galaxy Formation - Part Two - Comparison with N-Body Simulations. *Mon. Not. R. Astron. Soc.* , 271:676–+, December 1994.

[83] M. Davis, G. Efstathiou, C. S. Frenk, and S. D. M. White. The evolution of large-scale structure in a universe dominated by cold dark matter. *Astrophys. J.* , 292:371–394, May 1985.

[84] Z. Lukić, D. Reed, S. Habib, and K. Heitmann. The Structure of Halos: Implications for Group and Cluster Cosmology. *Astrophys. J.* , 692:217–228, February 2009.

[85] F. Lucchin and S. Matarrese. The effect of non-Gaussian statistics on the mass multiplicity of cosmic structures. *Astrophys. J.* , 330:535–544, July 1988.

[86] S. Colafrancesco, F. Lucchin, and S. Matarrese. The mass function from local density maxima - Groups and clusters of galaxies. *Astrophys. J.* , 345:3–11, October 1989.

[87] P. Coles and J. D. Barrow. Non-Gaussian statistics and the microwave background radiation.

Mon. Not. R. Astron. Soc. , 228:407–426, September 1987.

[88] W. H. Press and P. Schechter. Formation of Galaxies and Clusters of Galaxies by Self-Similar Gravitational Condensation. *Astrophys. J.* , 187:425–438, February 1974.

[89] J. A. Peacock and A. F. Heavens. Alternatives to the Press-Schechter cosmological mass function. *Mon. Not. R. Astron. Soc.* , 243:133–143, March 1990.

[90] S. Cole. Modeling galaxy formation in evolving dark matter halos. *Astrophys. J.* , 367:45–53, January 1991.

[91] J. R. Bond, S. Cole, G. Efstathiou, and N. Kaiser. Excursion set mass functions for hierarchical Gaussian fluctuations. *Astrophys. J.* , 379:440–460, October 1991.

[92] R. K. Sheth and G. Tormen. Large-scale bias and the peak background split. *Mon. Not. R. Astron. Soc.* , 308:119–126, September 1999.

[93] M. Maggiore and A. Riotto. The Halo Mass Function from Excursion Set Theory. I. Gaussian fluctuations with non-markovian dependence on the smoothing scale. *ArXiv e-prints*, March 2009.

[94] S. Matarrese, L. Verde, and R. Jimenez. The Abundance of High-Redshift Objects as a Probe of Non-Gaussian Initial Conditions. *Astrophys. J.* , 541:10–24, September 2000.

[95] M. Lo Verde, A. Miller, S. Shandera, and L. Verde. Effects of scale-dependent non-Gaussianity on cosmological structures. *Journal of Cosmology and Astro-Particle Physics*, 4:14–+, April 2008.

[96] P. Valageas. Mass function and bias of dark matter halos for non-Gaussian initial conditions. *ArXiv e-prints*, June 2009.

[97] M. Grossi, K. Dolag, E. Branchini, S. Matarrese, and L. Moscardini. Evolution of massive haloes in non-Gaussian scenarios. *Mon. Not. R. Astron. Soc.*, 382:1261–1267, December 2007.

[98] M. Grossi, L. Verde, C. Carbone, K. Dolag, E. Branchini, F. Iannuzzi, S. Matarrese, and L. Moscardini. Large-scale non-Gaussian mass function and halo bias: tests on N-body simulations. *Mon. Not. R. Astron. Soc.* , 398:321–332, September 2009.

[99] X. Kang, P. Norberg, and J. Silk. Can a large-scale structure probe cosmic microwave background-constrained non-Gaussianity? *Mon. Not. R. Astron. Soc.* , 376:343–347, March 2007.

[100] V. Desjacques and U. Seljak. Signature of primordial non-Gaussianity of ϕ^3 type in the mass function and bias of dark matter haloes. *Phys. Rev. D.* , 81(2):023006–+, January 2010.

[101] M. Maggiore and A. Riotto. The Halo Mass Function from Excursion Set Theory with a Non-Gaussian Trispectrum. *ArXiv e-prints*, October 2009.

[102] M. Maggiore and A. Riotto. The Halo Mass Function from Excursion Set Theory. II. The Diffusing Barrier. *ArXiv e-prints*, March 2009.

[103] M. Maggiore and A. Riotto. The Halo Mass Function from Excursion Set Theory. III. Non-Gaussian Fluctuations. *ArXiv e-prints*, March 2009.

[104] T. Y. Lam and R. K. Sheth. Halo abundances in the f_{nl} model. *Mon. Not. R. Astron. Soc.* , 398:2143–2151, October 2009.

[105] T. Y. Lam, R. K. Sheth, and V. Desjacques. The initial shear field in models with primordial local non-Gaussianity and implications for halo and void abundances. *Mon. Not. R. Astron. Soc.* , 399:1482–1494, November 2009.

[106] P. P. Avelino and P. T. P. Viana. The cloud-in-cloud problem for non-Gaussian density fields. *Mon. Not. R. Astron. Soc.* , 314:354–358, May 2000.

[107] K. T. Inoue and M. Nagashima. Analytic Approach to the Cloud-in-Cloud Problem for Non-Gaussian Density Fluctuations. *Astrophys. J.* , 574:9–18, July 2002.

[108] R. K. Sheth, H. J. Mo, and G. Tormen. Ellipsoidal collapse and an improved model for the number and spatial distribution of dark matter haloes. *Mon. Not. R. Astron. Soc.* , 323:1–12, May 2001.

[109] V. Desjacques. Environmental dependence in the ellipsoidal collapse model. *Mon. Not. R. Astron. Soc.* , 388:638–658, August 2008.

[110] S. Matarrese, F. Lucchin, and S. A. Bonometto. A path-integral approach to large-scale matter distribution originated by non-Gaussian fluctuations. *Astrophys. J. Lett.*, 310:L21–L26, November 1986.

[111] P. Catelan, F. Lucchin, and S. Matarrese. Peak number density of non-Gaussian random fields. *Physical Review Letters*, 61:267–270, July 1988.

[112] S. Borgani and S. A. Bonometto. Galaxy density in biased theories of galaxy origin. *Astron. Astrophys.* , 215:17–20, May 1989.

[113] S. Matarrese, F. Lucchin, A. Messina, and L. Moscardini. Non-Gaussian initial conditions in cosmological N-body simulations. III - Groups in Cold Dark Matter models.

Mon. Not. R. Astron. Soc. , 253:35–46, November 1991.

[114] C. Park, D. N. Spergel, and N. Turok. Large-scale structure in a texture-seeded cold dark matter cosmogony. *Astrophys. J. Lett.* , 372:L53–L57, May 1991.

[115] S. Borgani, P. Coles, L. Moscardini, and M. Plionis. The Angular Distribution of Clusters in Skewed CDM Models / Cold Dark Matter. *Mon. Not. R. Astron. Soc.* , 266:524–+, January 1994.

[116] H. Mathis, J. M. Diego, and J. Silk. The case for non-Gaussianity on cluster scales. *Mon. Not. R. Astron. Soc.* , 353:681–688, September 2004.

[117] J. Robinson and J. E. Baker. Evolution of the cluster abundance in non-Gaussian models. *Mon. Not. R. Astron. Soc.* , 311:781–792, February 2000.

[118] R. Stanek, A. E. Evrard, H. Böhringer, P. Schuecker, and B. Nord. The X-Ray Luminosity-Mass Relation for Local Clusters of Galaxies. *Astrophys. J.* , 648:956–968, September 2006.

[119] D. Nagai. The Impact of Galaxy Formation on the Sunyaev-Zel'dovich Effect of Galaxy Clusters. *Astrophys. J.* , 650:538–549, October 2006.

[120] W. A. Chiu, J. P. Ostriker, and M. A. Strauss. Using Cluster Abundances and Peculiar Velocities to Test the Gaussianity of the Cosmological Density Field. *Astrophys. J.* , 494:479–+, February 1998.

[121] K. Koyama, J. Soda, and A. Taruya. Constraints on a non-Gaussian (χ^2) cold dark matter model. *Mon. Not. R. Astron. Soc.* , 310:1111–1118, December 1999.

[122] J. Robinson, E. Gawiser, and J. Silk. Constraining Primordial Non-Gaussianity with the Abundance of High-Redshift Clusters. *Astrophys. J.* , 532:1–16, March 2000.

[123] A. J. Benson, C. Reichardt, and M. Kamionkowski. Statistics of Sunyaev-Zel'dovich cluster surveys. *Mon. Not. R. Astron. Soc.* , 331:71–84, March 2002.

[124] S. Sadeh, Y. Rephaeli, and J. Silk. Impact of a non-Gaussian density field on Sunyaev-Zeldovich observables. *Mon. Not. R. Astron. Soc.* , 368:1583–1598, June 2006.

[125] S. Sadeh, Y. Rephaeli, and J. Silk. Cluster abundances and Sunyaev-Zel'dovich power spectra: effects of non-Gaussianity and early dark energy. *Mon. Not. R. Astron. Soc.* , 380:637–645, September 2007.

[126] E. Sefusatti, C. Vale, K. Kadota, and J. Frieman. Primordial Non-Gaussianity and Dark Energy Constraints from Cluster Surveys. *Astrophys. J.* , 658:669–679, April 2007.

[127] C. Fedeli, L. Moscardini, and S. Matarrese. The clustering of galaxy clusters in cosmological models with non-Gaussian initial conditions: predictions for future surveys. *Mon. Not. R. Astron. Soc.* , 397:1125–1137, August 2009.

[128] M. Roncarelli, L. Moscardini, E. Branchini, K. Dolag, M. Grossi, F. Iannuzzi, and S. Matarrese. Imprints of primordial non-Gaussianities in X-ray and SZ signals from galaxy clusters. *ArXiv e-prints*, September 2009.

[129] J. Oukbir, J. G. Bartlett, and A. Blanchard. X-ray galaxy clusters: constraints on models of galaxy formation. *Astron. Astrophys.* , 320:365–377, April 1997.

[130] J. P. Henry. Measuring Cosmological Parameters from the Evolution of Cluster X-Ray Temperatures. *Astrophys. J.* , 534:565–580, May 2000.

[131] A. Amara and A. Refregier. Power spectrum normalization and the non-Gaussian halo model. *Mon. Not. R. Astron. Soc.* , 351:375–383, June 2004.

[132] R. Mandelbaum and U. Seljak. A robust lower limit on the amplitude of matter fluctuations in the universe from cluster abundance and weak lensing. *Journal of Cosmology and Astro-Particle Physics*, 6:24–+, June 2007.

[133] M. Kamionkowski, L. Verde, and R. Jimenez. The void abundance with non-gaussian primordial perturbations. *Journal of Cosmology and Astro-Particle Physics*, 1:10–+, January 2009.

[134] A. G. Doroshkevich. The space structure of perturbations and the origin of rotation of galaxies in the theory of fluctuation. *Astrofizika*, 6:581–600, 1970.

[135] H. Song and J. Lee. The Mass Function of Void Groups as a Probe of Primordial Non-Gaussianity. *Astrophys. J. Lett.* , 701:L25–L28, August 2009.

[136] R. K. Sheth and R. van de Weygaert. A hierarchy of voids: much ado about nothing. *Mon. Not. R. Astron. Soc.* , 350:517–538, May 2004.

[137] C. Carbone, L. Verde, and S. Matarrese. Non-Gaussian Halo Bias and Future Galaxy Surveys. *Astrophys. J. Lett.* , 684:L1–L4, September 2008.

[138] J. M. Colberg, F. Pearce, C. Foster, E. Platen, R. Brunino, M. Neyrinck, S. Basilakos, A. Fairall, H. Feldman, S. Gottlöber, O. Hahn, F. Hoyle, V. Müller, L. Nelson, M. Plionis, C. Porciani, S. Shandarin, M. S. Vogeley, and R. van de Weygaert. The Aspen-Amsterdam void finder comparison project. *Mon. Not. R. Astron. Soc.* , 387:933–944, June 2008.

[139] A. Dressler. Galaxy morphology in rich clusters - Implications for the formation and evolution of galaxies. *Astrophys. J.* , 236:351–365, March 1980.
[140] P. J. E. Peebles. The sequence of cosmogony and the nature of primeval departures from homogeneity. *Astrophys. J.* , 274:1–6, November 1983.
[141] N. A. Bahcall and R. M. Soneira. The spatial correlation function of rich clusters of galaxies. *Astrophys. J.* , 270:20–38, July 1983.
[142] A. A. Klypin and A. I. Kopylov. The Spatial Covariance Function for Rich Clusters of Galaxies. *Soviet Astronomy Letters*, 9:41–+, February 1983.
[143] B. Grinstein and M. B. Wise. Non-Gaussian fluctuations and the correlations of galaxies or rich clusters of galaxies. *Astrophys. J.* , 310:19–22, November 1986.
[144] A. P. A. Andrade, A. L. B. Ribeiro, and C. A. Wuensche. High order correction terms for the peak-peak correlation function in nearly-Gaussian models. *Astron. Astrophys.* , 457:385–391, October 2006.
[145] S. Matarrese and L. Verde. The Effect of Primordial Non-Gaussianity on Halo Bias. *Astrophys. J. Lett.* , 677:L77–L80, April 2008.
[146] J. M. Bardeen, J. R. Bond, N. Kaiser, and A. S. Szalay. The statistics of peaks of Gaussian random fields. *Astrophys. J.* , 304:15–61, May 1986.
[147] S. Cole and N. Kaiser. Biased clustering in the cold dark matter cosmogony. *Mon. Not. R. Astron. Soc.* , 237:1127–1146, April 1989.
[148] A. Slosar, C. Hirata, U. Seljak, S. Ho, and N. Padmanabhan. Constraints on local primordial non-Gaussianity from large scale structure. *Journal of Cosmology and Astro-Particle Physics*, 8:31–+, August 2008.
[149] N. Afshordi and A. J. Tolley. Primordial non-Gaussianity, statistics of collapsed objects, and the integrated Sachs-Wolfe effect. *Phys. Rev. D.* , 78(12):123507–+, December 2008.
[150] P. J. E. Peebles. An Isocurvature Cold Dark Matter Cosmogony. II. Observational Tests. *Astrophys. J.* , 510:531–540, January 1999.
[151] R. Y. Cen, J. P. Ostriker, D. N. Spergel, and N. Turok. A hydrodynamic approach to cosmology - Texture-seeded cold dark matter and hot dark matter cosmogonies. *Astrophys. J.* , 383:1–18, December 1991.
[152] L. Verde and S. Matarrese. Detectability of the Effect of Inflationary Non-Gaussianity on Halo Bias. *Astrophys. J. Lett.* , 706:L91–L95, November 2009.
[153] E. Hatziminaoglou, G. Mathez, J.-M. Solanes, A. Manrique, and E. Salvador-Solé. Major mergers of haloes, the growth of massive black holes and the evolving luminosity function of quasars. *Mon. Not. R. Astron. Soc.* , 343:692–704, August 2003.
[154] P. F. Hopkins, L. Hernquist, T. J. Cox, T. Di Matteo, P. Martini, B. Robertson, and V. Springel. Black Holes in Galaxy Mergers: Evolution of Quasars. *Astrophys. J.* , 630:705–715, September 2005.
[155] S. Bonoli, F. Shankar, S. White, V. Springel, and S. Wyithe. On merger bias and the clustering of quasars. *ArXiv e-prints*, August 2009.
[156] N. Bartolo, S. Matarrese, and A. Riotto. Signatures of primordial non-Gaussianity in the large-scale structure of the universe. *Journal of Cosmology and Astro-Particle Physics*, 10:10–+, October 2005.
[157] D. Wands and A. Slosar. Scale-dependent bias from primordial non-Gaussianity in general relativity. *Phys. Rev. D.* , 79(12):123507–+, June 2009.
[158] P. McDonald. Primordial non-Gaussianity: Large-scale structure signature in the perturbative bias model. *Phys. Rev. D.* , 78(12):123519–+, December 2008.
[159] N. Kaiser. Clustering in real space and in redshift space. *Mon. Not. R. Astron. Soc.* , 227:1–21, July 1987.
[160] A. J. S. Hamilton. Linear Redshift Distortions: a Review. In D. Hamilton, editor, *The Evolving Universe*, volume 231 of *Astrophysics and Space Science Library*, pages 185–+, 1998.
[161] H. A. Feldman, N. Kaiser, and J. A. Peacock. Power-spectrum analysis of three-dimensional redshift surveys. *Astrophys. J.* , 426:23–37, May 1994.
[162] U. Seljak. Extracting Primordial Non-Gaussianity without Cosmic Variance. *Physical Review Letters*, 102(2):021302–+, January 2009.
[163] P. McDonald and U. Seljak. How to evade the sample variance limit on measurements of redshift-space distortions. *Journal of Cosmology and Astro-Particle Physics*, 10:7–+, October 2009.
[164] A. Slosar. Optimal weighting in f_{NL} constraints from large scale structure in an idealised case. *Journal of Cosmology and Astro-Particle Physics*, 3:4–+, March 2009.
[165] U. Seljak, N. Hamaus, and V. Desjacques. How to Suppress the Shot Noise in Galaxy Surveys. *Physical Review Letters*, 103(9):091303–+, August 2009.

[166] N. Hamaus, et al. in preparation. 2010.

[167] Z. Fan and J. M. Bardeen. Distributions of Fourier modes of cosmological density fields. *Phys. Rev. D.* , 51:6714–6721, June 1995.

[168] A. J. Stirling and J. A. Peacock. Power correlations in cosmology: limits on primordial non-Gaussian density fields. *Mon. Not. R. Astron. Soc.* , 283:L99+, December 1996.

[169] E. Sefusatti and E. Komatsu. Bispectrum of galaxies from high-redshift galaxy surveys: Primordial non-Gaussianity and nonlinear galaxy bias. *Phys. Rev. D.* , 76(8):083004–+, October 2007.

[170] D. Jeong and E. Komatsu. Primordial Non-Gaussianity, Scale-dependent Bias, and the Bispectrum of Galaxies. *Astrophys. J.* , 703:1230–1248, October 2009.

[171] E. Gaztanaga. N-point correlation functions in the CfA and SSRS redshift distribution of galaxies. *Astrophys. J. Lett.* , 398:L17–L20, October 1992.

[172] E. Gaztanaga and J. Yokoyama. Probing the statistics of primordial fluctuations and their evolution. *Astrophys. J.* , 403:450–465, February 1993.

[173] F. R. Bouchet, M. A. Strauss, M. Davis, K. B. Fisher, A. Yahil, and J. P. Huchra. Moments of the Counts Distribution in the 1.2 Jansky IRAS Galaxy Redshift Survey. *Astrophys. J.* , 417:36–+, November 1993.

[174] C. M. Baugh, E. Gaztanaga, and G. Efstathiou. A comparison of the evolution of density fields in perturbation theory and numerical simulations - II. Counts-in-cells analysis. *Mon. Not. R. Astron. Soc.* , 274:1049–1070, June 1995.

[175] S. Luo and E. Vishniac. Bayesian approaches to testing the nature of primordial density fluctuation. *Astrophys. J.* , 443:469–478, April 1995.

[176] D. J. Croton, E. Gaztañaga, C. M. Baugh, P. Norberg, M. Colless, I. K. Baldry, J. Bland-Hawthorn, T. Bridges, R. Cannon, S. Cole, C. Collins, W. Couch, G. Dalton, R. De Propris, S. P. Driver, G. Efstathiou, R. S. Ellis, C. S. Frenk, K. Glazebrook, C. Jackson, O. Lahav, I. Lewis, S. Lumsden, S. Maddox, D. Madgwick, J. A. Peacock, B. A. Peterson, W. Sutherland, and K. Taylor. The 2dF Galaxy Redshift Survey: higher-order galaxy correlation functions. *Mon. Not. R. Astron. Soc.* , 352:1232–1244, August 2004.

[177] W. J. Frith, P. J. Outram, and T. Shanks. High-order 2MASS galaxy correlation functions: probing the Gaussianity of the primordial density field. *Mon. Not. R. Astron. Soc.* , 373:759–768, December 2006.

[178] T. Matsubara and Y. Suto. Nonlinear Evolution of Genus in a Primordial Random Gaussian Density Field. *Astrophys. J.* , 460:51–+, March 1996.

[179] P. Coles, L. Moscardini, M. Plionis, F. Lucchin, S. Matarrese, and A. Messina. Topology in two dimensions. IV - CDM models with non-Gaussian initial conditions. *Mon. Not. R. Astron. Soc.* , 260:572–588, February 1993.

[180] T. Matsubara and J. Yokoyama. Genus Statistics of the Large-Scale Structure with Non-Gaussian Density Fields. *Astrophys. J.* , 463:409–+, June 1996.

[181] C. Hikage, A. Taruya, and Y. Suto. Genus Statistics for Galaxy Clusters and Nonlinear Biasing of Dark Matter Halos. *Astrophys. J.* , 556:641–652, August 2001.

[182] C. Hikage, P. Coles, M. Grossi, L. Moscardini, K. Dolag, E. Branchini, and S. Matarrese. The effect of primordial non-Gaussianity on the topology of large-scale structure. *Mon. Not. R. Astron. Soc.* , 385:1613–1620, April 2008.

[183] J. R. Gott, III, D. C. Hambrick, M. S. Vogeley, J. Kim, C. Park, Y.-Y. Choi, R. Cen, J. P. Ostriker, and K. Nagamine. Genus Topology of Structure in the Sloan Digital Sky Survey: Model Testing. *Astrophys. J.* , 675:16–28, March 2008.

[184] J. B. James, M. Colless, G. F. Lewis, and J. A. Peacock. Topology of non-linear structure in the 2dF Galaxy Redshift Survey. *Mon. Not. R. Astron. Soc.* , 394:454–466, March 2009.

[185] J. N. Fry and E. Gaztanaga. Biasing and hierarchical statistics in large-scale structure. *Astrophys. J.* , 413:447–452, August 1993.

[186] X. Chen, A. Cooray, N. Yoshida, and N. Sugiyama. Can non-Gaussian cosmological models explain the WMAP high optical depth for reionization? *Mon. Not. R. Astron. Soc.* , 346:L31–L35, December 2003.

[187] P. P. Avelino and A. R. Liddle. Cosmic reionization constraints on the nature of cosmological perturbations. *Mon. Not. R. Astron. Soc.* , 371:1755–1759, October 2006.

[188] D. Crociani, L. Moscardini, M. Viel, and S. Matarrese. The effects of primordial non-Gaussianity on the cosmological reionization. *Mon. Not. R. Astron. Soc.* , 394:133–141, March 2009.

[189] M. Viel, E. Branchini, K. Dolag, M. Grossi, S. Matarrese, and L. Moscardini. Primordial non-Gaussianities in the intergalactic medium. *Mon. Not. R. Astron. Soc.* , 393:774–782, March 2009.

[190] S. Ho, et al. in preparation. 2010.

[191] J. E. Gunn and B. A. Peterson. On the Density of Neutral Hydrogen in Intergalactic Space. *Astrophys. J.* , 142:1633–1641, November 1965.

[192] E. Komatsu, K. M. Smith, J. Dunkley, C. L. Bennett, B. Gold, G. Hinshaw, N. Jarosik, D. Larson, M. R. Nolta, L. Page, D. N. Spergel, M. Halpern, R. S. Hill, A. Kogut, M. Limon, S. S. Meyer, N. Odegard, G. S. Tucker, J. L. Weiland, E. Wollack, and E. L. Wright. Seven-Year Wilkinson Microwave Anisotropy Probe (WMAP) Observations: Cosmological Interpretation. *ArXiv e-prints*, January 2010.

[193] P. Vielva and J. L. Sanz. Constraints on f_nl and g_nl from the analysis of the N-pdf of the CMB large scale anisotropies. *ArXiv e-prints*, October 2009.

[194] J. A. Frieman and E. Gaztañaga. The Projected Three-Point Correlation Function: Theory and Observations. *Astrophys. J. Lett.* , 521:L83–L86, August 1999.

[195] R. Scoccimarro, H. A. Feldman, J. N. Fry, and J. A. Frieman. The Bispectrum of IRAS Redshift Catalogs. *Astrophys. J.* , 546:652–664, January 2001.

[196] G. V. Kulkarni, R. C. Nichol, R. K. Sheth, H.-J. Seo, D. J. Eisenstein, and A. Gray. The three-point correlation function of luminous red galaxies in the Sloan Digital Sky Survey. *Mon. Not. R. Astron. Soc.* , 378:1196–1206, July 2007.

[197] E. Gaztañaga, A. Cabré, F. Castander, M. Crocce, and P. Fosalba. Clustering of luminous red galaxies - III. Baryon acoustic peak in the three-point correlation. *Mon. Not. R. Astron. Soc.* , 399:801–811, October 2009.

[198] J. A. Willick. Constraints on Primordial Non-Gaussianity from the High-Redshift Cluster MS 1054-03. *Astrophys. J.* , 530:80–95, February 2000.

[199] R. Jimenez and L. Verde. Implications for primordial non-Gaussianity (f_{NL}) from weak lensing masses of high-z galaxy clusters. *Phys. Rev. D.* , 80(12):127302–+, December 2009.

[200] B. Sartoris, S. Borgani, C. Fedeli, S. Matarrese, L. Moscardini, P. Rosati, and J. Weller. The potential of X-ray cluster surveys to constrain primordial non-Gaussianity. *ArXiv e-prints*, March 2010.

[201] D. Jeong, E. Komatsu, and B. Jain. Galaxy-CMB and galaxy-galaxy lensing on large scales: Sensitivity to primordial non-Gaussianity. *Phys. Rev. D.* , 80(12):123527–+, December 2009.

[202] C. Fedeli and L. Moscardini. Cosmic shear statistics in cosmologies with non-Gaussian initial conditions. *ArXiv e-prints*, December 2009.

[203] M. Takada and B. Jain. Cosmological parameters from lensing power spectrum and bispectrum tomography. *Mon. Not. R. Astron. Soc.* , 348:897–915, March 2004.

[204] Y. Gong, X. Wang, Z. Zheng, and X.-L. Chen. Primordial non-Gaussianity from LAMOST surveys. *Research in Astronomy and Astrophysics*, 10:107–115, February 2010.

[205] E. Sefusatti, M. Liguori, A. P. S. Yadav, M. G. Jackson, and E. Pajer. Constraining running non-gaussianity. *Journal of Cosmology and Astro-Particle Physics*, 12:22–+, December 2009.

[206] C. Carbone, O. Mena, and L. Verde. Cosmological Parameters Degeneracies and Non-Gaussian Halo Bias. *ArXiv e-prints*, March 2010.

[207] M. Oguri. Self-Calibrated Cluster Counts as a Probe of Primordial Non-Gaussianity. *Physical Review Letters*, 102(21):211301–+, May 2009.

[208] C. Cunha, D. Huterer, and O. Dore. Primordial non-Gaussianity from the covariance of galaxy cluster counts. *ArXiv e-prints*, March 2010.